Capturing geological uncertainty in salt cavern developments for hydrogen storage: Case study from Southern North Sea.

i. Hector George Barnett*[1], Mark T. Ireland[1], Cees Van der Land[1]

ii. [1] Earth Ocean and Planetary Science Group, School of Natural and Environmental Sciences, Drummond Building, Newcastle University, Newcastle Upon-Tyne NE1 7RU

iii. *Corresponding Author Email Address: h.barnett2@ncl.ac.uk

PREPRINT STATEMENT

Keywords: Energy Storage, Salt Caverns, Hydrogen Storage, Geological modelling, Gas Storage, Energy Systems

Abstract

Future energy systems that have a greater contribution from renewable energy will require long-duration energy storage to optimise the integration of renewable energy sources, hydrogen is an energy vector that could be utilised for this. Grid-scale underground natural gas storage is already in operation in solution-mined salt caverns, where individual cavern capacities are ~25 - 275 GWh. To date, salt caverns have been restricted to being developed onshore, however in some offshore geographic locations, such as the UK Continental Shelf, there are extensive evaporite layers which have the potential for storage development. Existing capacity estimates for offshore areas, have relied upon generalised regional geological interpretations, frequently do not incorporate site-specific structural and lithological heterogeneities, use static cavern geometries, and use methodologies that are deterministic and not repeatable.

We have developed a stochastic method for identifying viable salt cavern locations and estimating conceptual clusters' storage capacity. The workflow incorporates the principle geomechanical constraints on cavern development, captures limitations from internal evaporite heterogeneities, and uses the ideal gas law to calculate the volumetric capacity. The model can accommodate either fixed cavern geometries or geometries that vary per site depending on the thickness of salt. The workflow also allows for surface restrictions to be included. By using a stochastic method, we quantify the uncertainties for storage capacity estimates and cavern placement across defined regions of interest. The workflow is easily adaptable allowing for users to consider multiple geological models or evaluate the impact of interpretations of varying resolutions.

We illustrate the use of the model for four different areas and geological models across the Southern North Sea of the United Kingdom:

1) Basin Scale (58,900 km^2) - predicting >61.9 PWh's of hydrogen storage capacity with over 199,000 possible cavern locations.
2) Sub-Regional Scale (24,800 km^2) – predicting >12.1 PWh's of hydrogen storage capacity with over 36,000 possible cavern locations.
3) Block Specific – Salt Wall (79.8km^2) - predicting >731 TWh's of hydrogen storage capacity with over 400 possible cavern locations.
4) Block Specific – Layered Evaporite (225 km^2) - predicting >419 TWh's of hydrogen storage capacity with over 460 possible cavern locations.

When we incorporate conceptual development constraints, we identify a cavern cluster in the layered evaporite study, consisting of 22 salt caverns in an area of 7 km^2 that could store 67% (26.9 TWh) of the energy needs estimated for the UK in 2050 (~40 – 120 TWh). Our workflow enables reproducible and replicable assessments of site screening and storage capacity estimates. A workflow built around these ideals allows for fully transparent results. We compare our results against other similar studies in literature and find that often highly cited papers have inappropriate methodologies and hence capacities.

1. Introduction

Long-duration energy storage (LDES) will be a vital feature in future energy systems (McNamara et al., 2022, Smdani et al., 2022). As renewable and low-carbon energy displaces fossil fuels there will be a requirement to accommodate the increased variability in supply that comes with this transition (Dowling et al., 2020). LDES allows for the management of grid imbalances that arise from both the variable supply of renewable energy and the variability on the demand side, while improving the overall flexibility and reliability of the energy system (Kueppers et al., 2021, Sepulveda et al., 2021). There are three principal mechanisms for geological LDES: mechanical (compressed air or solid weight), thermal, and chemical energy storage (hydrogen, ammonia, natural gas) (Bauer et al., 2013, Shan et al., 2022). Chemical storage is often considered the most versatile option of these three, as the energy storage medium can also be transported and used with relative ease and with a low energy loss (<0.1% vs 5% for high voltage energy cables), over long distances, adding to the flexibility of the energy system as a whole (Calado and Castro, 2021).

Subsurface formations have proven to be suitable storage containers for geological scales of time, as evidenced by the occurrence of natural hydrocarbon accumulations (Lokhorst and Wildenborg, 2006). The subsurface has already been utilized for many decades for the storage of natural gas. The Rough gas storage field, for example, located offshore UK, has been in operation since 1985 (with a 5-year hiatus from 2017 - 2022) with the capacity to store 54 BCF of natural gas (Centrica, 2023), or in Cheshire, UK, Storengy operates a salt cavern cluster consisting of 28 caverns with the ability to store 14 BCF of gas (Eising et al., 2021). Hydrogen has also been stored within the subsurface, the Spindletop salt caverns cluster in Texas, USA, for example, which stored 5 BCF (≈ 1450 GWh) of natural gas, was converted to store 274 GWh of hydrogen (Bérest et al., 2021). Compared with other methods of LDES, such as Li-Po batteries and pumped-hydro, subsurface geological storage provides several advantages, such as, greater capacities, small surface footprint, low specific investments and operating costs, operational timespans for over 30 years, and increased security (Crotogino et al., 2017). There are two differing storage methods within the subsurface, porous media (e.g. saline aquifers and abandoned hydrocarbon fields) or salt caverns (Evans, 2007, Bauer et al., 2013). Salt caverns for hydrogen storage are the technology of investigation within this study, as, while research has been undertaken on hydrogen storage in porous media such as Heinemann et al. (2018),Heinemann et al. (2021) and Hassanpouryouzband et al. (2022), storage of hydrogen in porous media has yet to be deployed, whereas there are several salt cavern clusters storing hydrogen currently in operation.

Salt caverns are solution mined voids within a evaporitic (salt) layers (Warren, 2006, Tarkowski and Czapowski, 2018). They range volumetrically from 70,000 m^3 (e.g Teesside, UK (HyUnder, 2013)) to 17,000,000 m^3 (Texas (Leith, 2000)). Salt caverns are an established technology having been in use since 1960's for storing gas (Allen, 1972). Hydrogen has been stored within salt caverns since the early 1970's for use in chemical industry, with the first site located in Teesside, UK (Landinger and Crotogino, 2007, Caglayan et al., 2020, François, 2021) and other select locations elsewhere in the world (Figure. 1). Recent published work on salt cavern volumetrics has focused on onshore areas, and frequently at a country-wide scale analysis for capacity estimates and cavern placement (e.g. Caglayan et al. (2020) and Williams et al. (2022)), modelled capacity estimates across whole basins greatly exceed the estimated requirements for LDES. The estimates make use of coarse resolution geological models and are not able to capture the geological complexity of both the salt layers, and the overlying geological complexity. Simplified, or basic geological models may not reliably estimate cavern placement options, and their storage capacity. In the UK to date, there has not been a systematic assessment of the geological constraints on offshore salt cavern development. However, offshore salt caverns are not outside technological feasibility (Costa et al., 2017). One of the possible benefits from offshore storage is the co-location of storage next to offshore windfarms, or pre-existing pipelines, developing both a hub of energy production and storage. Salt caverns are typically developed in clusters (Gillhaus., 2007) and the work here could be considered as the basis for pre-feasibility studies of cavern placement options.

We demonstrate the robustness and flexibility of our methodology for the offshore of the UK. The UK is currently undergoing a shift in the supply of energy to meet its 2050 net-zero obligations, with installed wind power capacity in 2023 reaching 27.9 GW (Staffell et al., 2023). For 100% renewable penetration by 2035 in the UK, Cárdenas et al. (2021) found that with the optimum mix of renewable technologies and allowing for over-generation, the UK would require ~42 TWh of LDES, far lower than the suggested 115 TWh needed if no over generation is allowed. The UK's Electricity System Operator (2023) states that a whole energy system transformation by 2050 would require the UK to have 56 TWh of hydrogen storage by 2050. Without the utilisation of LDES within the energy mix it will be difficult for the UK to achieve its legislated net-zero carbon goals (King et al., 2021). Geological storage is currently the most viable option for LDES within the UK as: 1) there are a number of possible location options distributed across the UK, and the location of storage is an important consideration in the whole system (Sunny et al., 2020); 2) pre-existing oil and gas infrastructure could be repurposed to reduce capital expenditure associated with LDES scale up (Oil and Gas Authority, 2021); 3) Geological storage is estimated to currently be one of the lowest cost LDES options available (Hunter et al., 2021).

Figure 1.

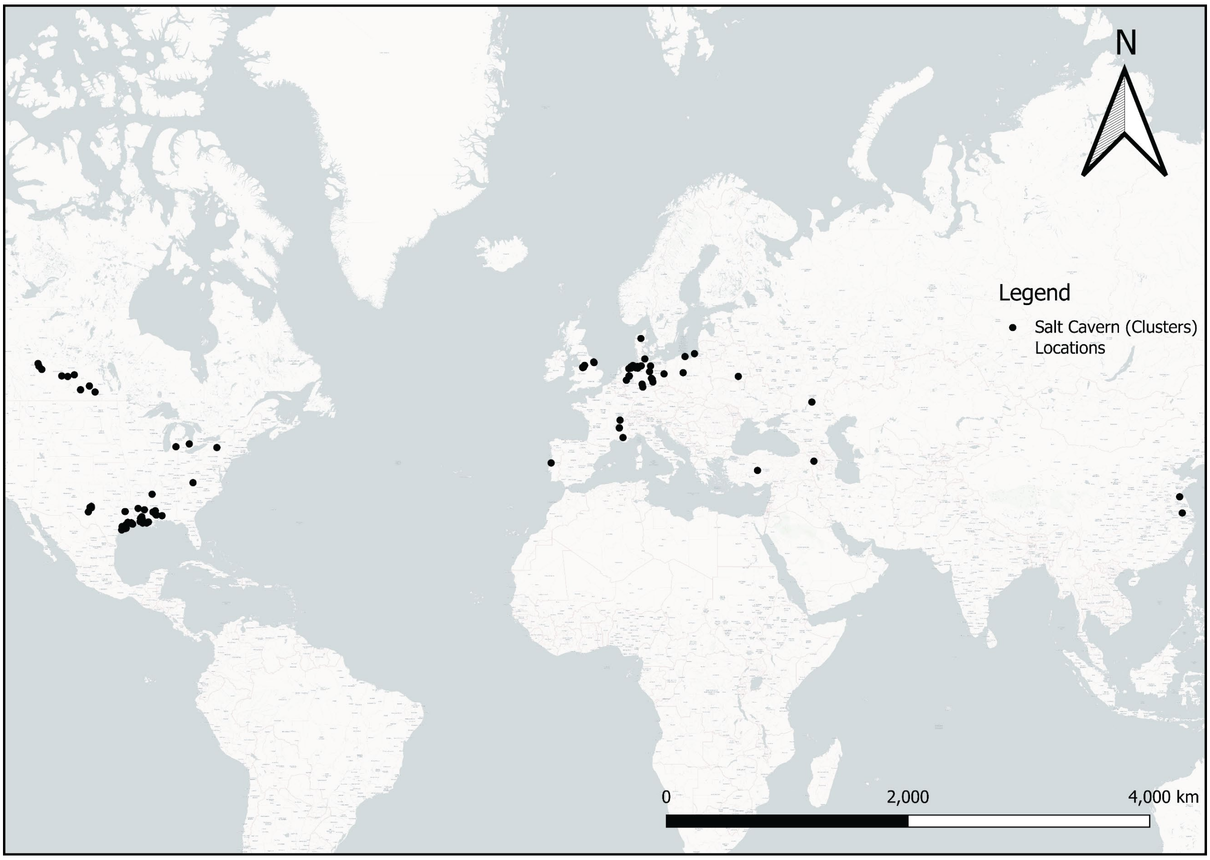

Figure. 1 – Global location map of current salt cavern sites. Note, all salt cavern location sites are currently located onshore. Data from International Gas Union (2023).

1.1 Area of Interest

We focus on the Southern North Sea area of the UKCS due to the data availability, geological suitability, and possible future demand for hydrogen storage within the area. Four areas of interest (AoIs) are defined within our study (Figure. 2) to consider the potential locations and capacity for salt caverns for hydrogen storage within Zechstein supergroup. The Zechstein supergroup is a Late Permian-aged layered evaporite sequence deposited during the Lopingian (Peryt et al., 2010), it is laterally extensive, and, across large areas exceeds 750 m in thickness. It is located within both the North Permian and South Permian Basins of Europe, where it extends from onshore the eastern coast of the UK, across to western Poland

(Glennie, 1998). The Zechstein Supergroup is found as both layered and structured salt throughout both basins, with most of the current understanding coming from hydrocarbon exploration and development, where it is important for trapping mechanisms and sealing reservoir intervals (Glennie, 1998, Strozyk, 2017, Doornenbal et al., 2019, Grant et al., 2019). The Zechstein's deposition as a layered evaporite sequence is typically divided into five cycles, however the nomenclature used frequently varies depending on regional location and environment of deposition (Johnson et al., 1993). The internal heterogeneity of the Zechstein varies in complexity across the Southern North Sea due to the Zechstein's mobility from halokinesis (Barnett et al., 2023).

Figure. 2

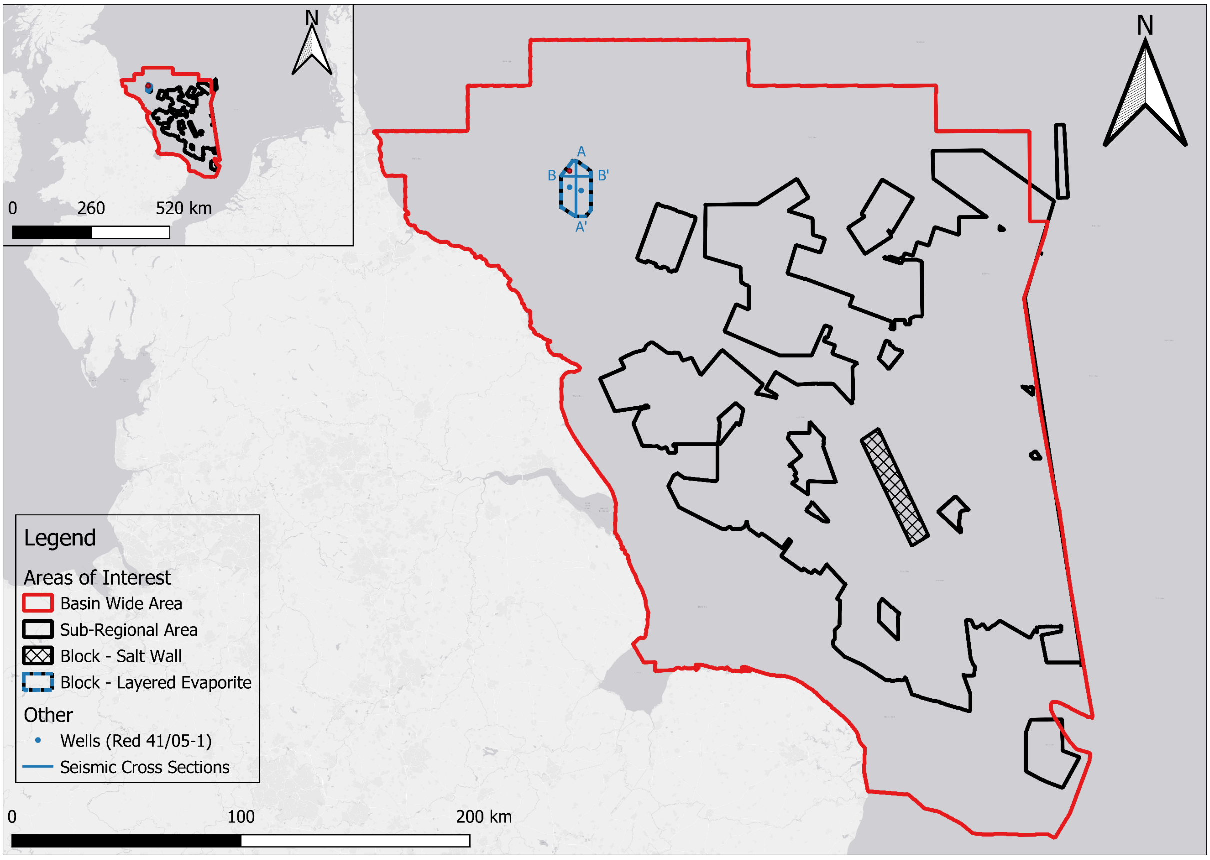

Figure. 2 – Location map of areas of interest (AoIs), offshore East coast of the UK. AoI locations are labelled and shown on the map. Well data used in the 'Block – Layered Evaporite' area is marked on, as well as seismic cross sections (Figure. 4 and Appendix. 3). Map 2, (top left) details the extent of the study areas in respect to the whole of the UK and Northern Europe.

2. Methodology

2.1 Workflow

The workflow in this study uses a geological model as the input and determines an idealised cavern layout and calculates the resulting working hydrogen storage capacity (Appendix. 1). Due to the inherent uncertainty associated with geological models, the method accommodates both deterministic and stochastic inputs. The workflow is agnostic to the resolution of the input geological models, recognising that the availability of data varies by area. The method can incorporate stochastic inputs in which case the workflow is run as a Montecarlo simulation, capturing the inherent uncertainty of the geological model. The workflow is a robust and repeatable method to determine the placement of salt caverns and calculate the hydrogen storage capacity. The workflow can be set to optimise for either cavern number or capacity, allowing for idealised utilisation of the area of interest.

The workflow initially removes areas of the geological model that have been determined as unsuitable based on the set parameters (Appendix. 1). The suitability of these areas for cavern placement is treated as binary condition, either suitable or not. It is possible to incorporate surface constraints, such as roads or population areas in onshore areas, or energy infrastructure offshore. Buffers can be applied to these features, which then determine a set distance for caverns to be placed.

The depth to geological formations can be constrained using seismic and well data, where seismic is used to interpret between the depth calibrated measurements from wells. As a result, depths in geological models have an inherent level of uncertainty. We accounted for this by using a uniform distribution calculated from the residual depth values calculated during the depth conversion process. The largest residual value from the depth conversion process was calculated as a percentage and set both the positive and negative limits of the uniform distribution. As depth uncertainty can be either positive or negative, setting the maximum residual to limit the uniform distribution (E.g., -10% and +10%) allows the workflow to account for depth uncertainty.

The workflow assumes that every grid cell within the geological model which has not been removed is a viable location for cavern placement. The height-to-diameter ratio at each viable location is determined by using the salt thickness at that location (Appendix. 1, Equation. 1). From the salt thickness and height-to-cavern ratio, a cavern geometry is determined (Appendix.1 Equations 2 - 6). If a fixed cavern geometry is used, then the pre-set maximum cavern height and cavern diameters are used instead. The shallowest a cavern can be emplaced in salt is 500 m (Warren, 2006, Caglayan et al., 2020, Tan et al., 2021), if a possible cavern location is in very shallow salt <500 m, it is checked to see if the salt is deeper than 500 m and has sufficient thickness beyond 500 m depth than the minimum cavern geometrical requirements. If so, a viable cavern is placed at 500 m deep. This optimisation allows for higher operating pressures, and hence higher hydrogen capacities in areas of shallow but thick salt (Appendix.1, Equation. 12).

The minimum distance between cavern mid points (buffer distance, Figure. 3) is then determined to establish the viable combination of adjacent cavern locations (Appendix. 1, Equation. 7) and is a simplified approach to account for the geomechanical requirements for stability between adjacent caverns (Caglayan et al., 2020, Ma et al., 2022). Where the grid cell spacing is greater than the buffer distance between caverns then there will be overlap between buffers. To determine a layout where there is no overlap of buffers the workflow iterates horizontally through the array of viable cavern locations starting at 0,0 (top left), plots a cavern, checks to see if the buffer overlaps with another caverns' buffer, and if it does not, keeps it, if it does, it is deemed unviable and removed. Further explanation of how this works can be seen in the Appendix under 'cavern best fit algorithm'. This methodology optimally packs the caverns within the areas viable for cavern placement.

The volume for each cavern is then calculated, (Appendix. 2, Equation. 8). For caverns with a height-to-diameter ratio of < 1, an ellipsoid shape was assumed for the volume (Appendix. 1, Equation. 8b), as pill geometries become ellipsoids with a height-to-diameter of <1. The volume for the cavern will depend on its planned geometrical shape. Our workflow uses pill geometries for the 3D cavern shape (Figure. 3), as these are the most stable and have the lowest stress risk (Ozarslan, 2012) (Appendix. 1, Equation. 8).

Figure. 3

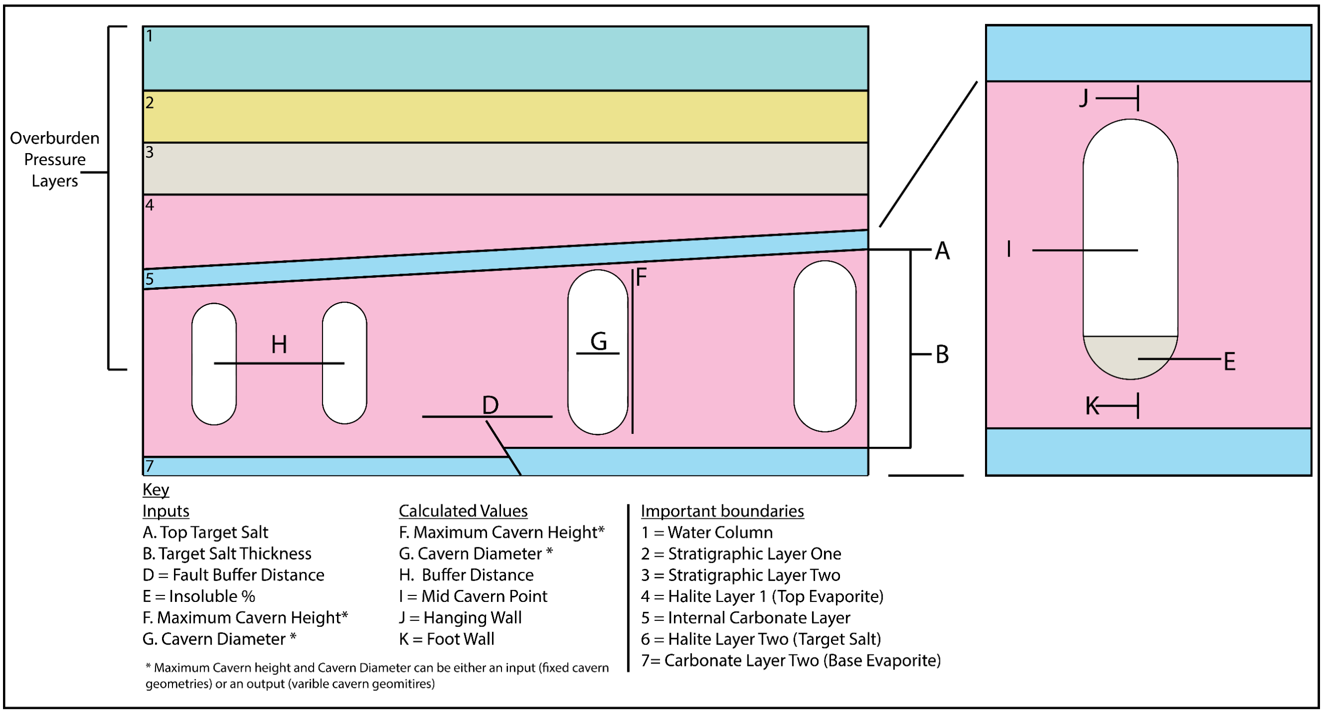

Figure. 3- Cartoon schematic geological cross-section of emplaced salt caverns (Not to scale). Important parameters (both inputs and calculations) for characterizing a salt cavern site have been labelled A – k, and overburden characterization 1 - 7. The right diagram shows an individual cavern and the parameters considered for individual cavern placement.

Remaining are all viable cavern locations within the area with correct spacing and geometries for the salt present. Lithostatic pressure for the mid cavern depth are calculated as they determine the cavern operating pressure. A simple 1D layer cake approach can be taken for calculating lithostatic pressure (Appendix. 1, Equation. 9) depending on data available (Section 2.2.3). For layer cake models, the same depth uncertainty is applied to that of the salt depth and thickness surfaces. An uncertainty can also be applied to the density of the overburden layers. Internal cavern temperatures are then calculated from a set geothermal gradient (Appendix. 1, Equation. 10, Section 2.2.2). The cavern volume is then adjusted to account for the insoluble content that is present within the salt (Appendix. 1, Equation. 11, Section 2.2.1), a simple % may be used or a distribution derived from well data.

Individual cavern hydrogen capacity is then calculated using the ideal gas law (Appendix. 1, Equation. 12). 60% of the lithostatic pressure at mid cavern depth is used to calculate the working capacity as a cushion gas of 20% is required to maintain cavern integrity and a maximum pressure inside caverns is set at 80% to avoid exceeding the fracture gradient (Ozarslan, 2012, Caglayan et al., 2020, Muhammed et al., 2022). Once the individual capacity of each cavern is known, the energy capacity for the whole area or a cavern cluster can be calculated (Appendix. 1, Equation. 13). The energy capacity calculations are modifiable to allow for different energy vectors, such as natural gas, compressed air, or other gases.

From the Monte Carlo simulation, p10, p50 and p90 values can be calculated. The outputs from this workflow allow not only for numerical capacity and cavern number but also the geospatial data.

2.2 Model Parameters

2.2.1 Insoluble Content

Extensive data from across the UK sector of the Southern North Sea's South Permian Basin was used for calculating the range of insoluble contents. The Z2 Stassfurt halite was the chosen Zechstein salt layer for which to calculate insolubilities for as it is typically the thickest salt unit within the South Permian Basis and the most likely to have cavern emplaced within it. It was hence decided that the distribution to be used for insolubility content was that of the Z2 Stassfurt halite from the whole of Southern North Sea basins (Appendix - Distributions).

Insoluble content was calculated from well logs as:

*Equation A: Insoluble content % = (Length insoluble lithology in evaporite stratigraphy / total length of evaporite stratigraphy) *100*

2.2.2 Temperature

Bottom hole temperatures were examined for all wells that had available data within the South Permian Basin from the CGG Geothermal Database (see Data Availability). Geothermal gradients were calculated from all the wells within the Basin Wide Area AoI (Figure. 2) within the geothermal database. From these calculated gradients, minimum and maximum gradients were extracted. The minimum maximum values set the bounds of a uniform distribution for geothermal gradients to use in the calculation of mid-cavern temperature (Appendix 1). The geothermal gradient was then used in Equation B to calculate cavern temperature. A sea floor temperature of 12 c° was assumed (Department for Environment Food and Rural Affairs, 2014).

*Equation B: Mid Cavern Temperature = Sea bed temperature + (Mid Cavern depth below sea floor * Geothermal gradient)*

2.2.3 Overburden Pressure

Two separate approaches for this were taken dependent on data available. 1) For areas where data for the above layers of the overburden were available as well as density data, a layer cake approach was used (Appendix. 1, Equation. 9). Due to the geological surfaces being used for thickness calculations and affected by the uncertainty in the depth conversion, these values were modified to the same uncertainty distribution that had been applied to the geological surfaces. Bulk density well logs were used to calculate the average densities for each of the geological layers in Appendix.1 Equation 9. These values were also subject to a certain level of uncertainty, so to account for this it was decided that a uniform distribution of +-10% was applied to the densities on each model run. This was not applied for the water column layer, instead, a constant value of 1024 Kg/m^3 was applied.

2) For areas where the data was not available to make a layer cake model, a simple 2-layer depth/gradient approach was used which accounted for both the water column and rock overburden separately. The gradient of the rock overburden was calculated from the average overburden density, a value of 1000 kg/m3 assumed for the water column and the depth taken from the cavern mid-point. (Appendix. 1, Equation. 9b).

2.3 Well and Seismic Data Interpretation Methodology

2.3.1 Well data interpretation.

Petrophysical logs were interpreted to distinguish different lithologies and hence different stratigraphic intervals. A combination of gamma-ray, sonic, and density logs were used alongside the supplied site geological descriptions and cuttings from the wells. For each well lithologies were interpreted. These applied well tops were quality controlled against the NSTA well top database and onsite geological reports for the well. For the Zechstein supergroup stratigraphy, however, lithologies were applied to the highest resolution allowed by the petrophysical logging tools. This resolution varies depending on the type of logging tool used;

however, it typically ranges from 1 – 5 m (Bourke et al., 1989). Following this, well-tops were applied for the intra Zechstein stratigraphy, using the same QC as used for the non-Zechstein stratigraphy. This well interpretation allowed for the interpretation of the key geological horizons within the seismic data.

2.3.2 Seismic Well Tie

Synthetic-seismic well ties were generated to correlate the interpreted stratigraphic boundaries from the well data that was in the depth domain (m) to the seismic data that was in the time domain (ms). Synthetic traces were generated using a 35hz ricker wavelet and extracted wavelets. These were compared with the original seismic data and the best match selected to be used. The wells were bulk shifted vertically to assure the most suitable time-depth match between well and seismic data, the top Zechstein seismic reflection was aimed to be matched by the bulk shifting process.

2.3.4 Seismic Data Interpretation

The reflections identified as key stratigraphic boundaries were then interpreted on the seismic data. Reflections of stratigraphic boundaries were initially mapped at intervals of 25 m in both the crosslines and inlines of the seismic data. Once suitable coverage of the area had been achieved, 3D auto tracking was used to complete the interpretation surface. If areas were not mapped by the auto-tracking, they were manually remapped in smaller increments and then re-autotracked. This process was repeated until suitable interpretations of each key reflection had been achieved. From these reflection interpretation horizons, surfaces were generated, the surfaces had a grid spacing of 50 x 50 m and used a convergent gridding algorithm. This process produced seamless surfaces.

Geological faults were mapped within the seismic data. To accomplish this, the view of the seismic data was set perpendicular to the direction of the fault plane, and the visible fault line mapped. Intersection intervals of 25 m were used, with the view of the seismic data being re-orientated if the fault orientation changed. Faults were mapped until they could not be perceived anymore within the seismic data.

2.3.5 Seismic Depth Conversion

Depth conversion is required where seismic data are in the time domain since all calculations used to determine cavern placement and geometry require depth as a constraint. To depth convert we follow a standard approach of using geophysical logs to determine the velocity structure in the subsurface. This is subsequently used to determine interval velocities for the layers within the geological model. Time-depth relationship data was extracted from wells within the area and generated time surfaces used at the identified velocity interval. The model generally has residuals <10 %. For a complete description of the depth conversion method please see the data repository.

3. Data and Interpretation

3.1 Basin Wide Salt Depth Model

The basin wide depth model covers an area of 58,904 km^2 (Figure. 2). The surfaces used in the model have a grid cell size of 250 m, the lowest resolution of depth models used. The surfaces were from are from the ‘NSTA and Lloyd's Register SNS Regional Geological Maps (Open Source)’ dataset and available from the NSTA public open data repository (https://opendata-nstauthority.hub.arcgis.com/explore). No information was supplied regarding depth uncertainty. We assume a 10% depth uncertainty.

3.2 Sub Regional Salt Depth Model

The depth surfaces for the sub regional salt depth model are from Barnett et al. (2023) and cover 25,000 km^2 (Figure. 2). The surfaces are from the interpretation of a regionally extensive 3D seismic volume of the Southern North Sea (OA__2019seis0001a), with top and base

Zechstein surfaces having already been converted from the time to depth domain. The grid cell size is 50 m. The depth surfaces have a 5% uncertainty associated with them.

3.3 Block Specific

Blocks, when referring to the offshore energy industry, define set areas in which licences have been granted for specific activities, such as oil and gas exploration, or more recently, carbon capture and storage. Gas storage licences are also awarded as blocks from the UK's North Sea Transition Authority, with Centrica being awarded a licence for the Rough Gas storage site in 2022 (North Sea Transition Authority, 2022). Exploration blocks in the Southern North Sea are on average 115 km^2, with the largest being 250 km^2. We aimed to mimic these spatial constraints when applying our workflow, as it is likely that licences and areas for gas storage in salt caverns will be granted in a similar manner by the North Sea Transition Authority.

3.3.1 Salt Wall Salt Depth Model

The depth surfaces from the salt wall cover an area of 420 km^2 (Figure. 2). It is located on a structure often referred to as the Audrey salt wall (Elam, 2007), which trends NNW – SSW in the UK sector of the South Permian Basin. The depth surfaces were extracted from the Sub regional depth model, and thus the grid cell sizing of 50 m and depth uncertainty of 5% remain the same.

3.3.2 Layered Evaporite Salt Depth Model

The layered evaporite salt depth model covered an area of 225 km^2 (Figure. 2). It is located at the northern edges of the South Permian Basin, just south of the Mid-North Sea High (Figure. 2). Seismic survey MA933F0002 was used to interpret top and base target salt, and other major stratigraphic reflections for the area (Table. 1). The reflection chosen as top target salt was the top of the Stassfurt halite and base target salt was base Stassfurt halite because the thickest and most homogenous section of halite was at this section in the interpreted well data (Figure. 4, 5). Two-way time surfaces were created as described in section 2.3.4. As the surfaces were in two-way time, they had to be depth converted. The depth conversion model used 5 layers (All those in table 5, excluding base Zechstein) and time-depth relationship data was taken from 2 wells within the area (See Data Repository). Our depth conversion model ended up with an average residual of 7% at the top of the target salt unit. Further information regarding the depth conversion process can be seen in the Data Repository. The final depth surfaces had a grid cell size of 50 m, and a residual uncertainty of 7%. Within the Stassfurt halite there were heterogeneities observed that were interpreted to be none-halite (insoluble) lithologies. These heterogeneities were difficult to interpret on seismic data due to the seismic reflections within the area abruptly terminating and being noisy. The area in which these heterogeneities were observed was instead mapped using seismic time slice views within the Stassfurt halite.

Figure. 4

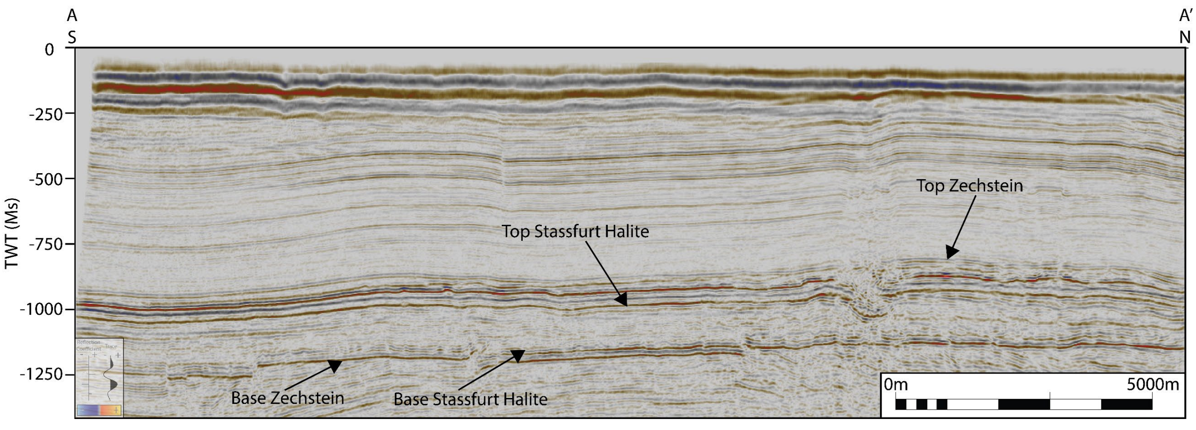

A) Example seismic cross section from the ‘Block – Layered Evaporite’ AoI (Seismic Survey MA933F0002), running North to South, A – A' (Figure. 2), in TWT, key reflections have been marked on.

Geological Horizon - Mapped
Seabed
Base Bunter Sandstone
Top Zechstein (Base bunter Shale)
Top Stassfurt Halite
Base Stassfurt Halite (above basal polyhalite reflection)
Base Zechstein

Table 1 – Key stratigraphic surfaces used for the layered evaporite geological model.

Figure. 5

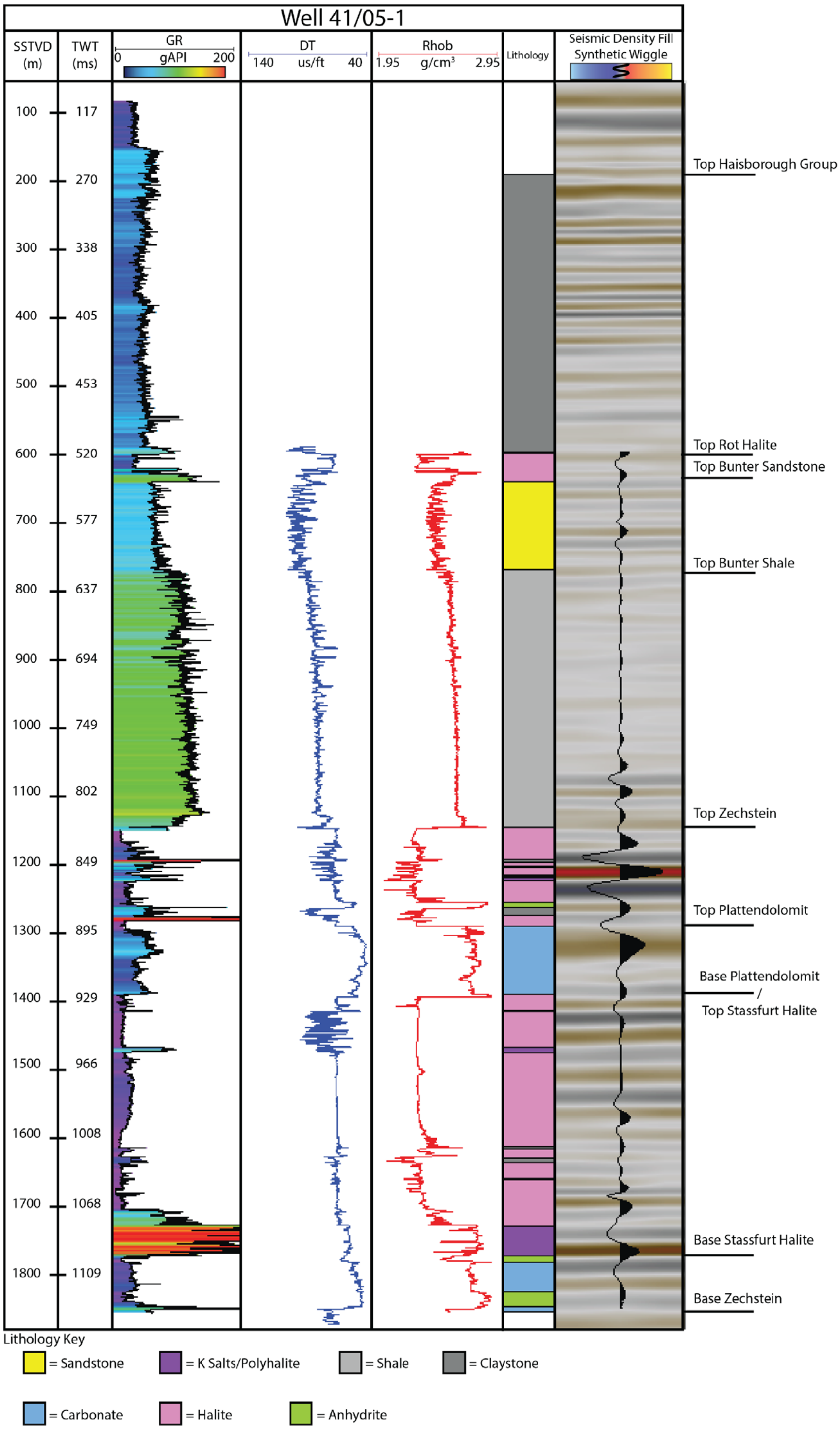

Figure 5 – Petrophysical logs (well 41/05-1, Figure. 2), GR (gamma-ray), DT (sonic), Rhob (density), interpreted lithology log is present. Calculated synthetic seismic wiggle overlying seismic trace from seismic survey MA933F002 and interpreted key stratigraphic boundaries.

3.4 Geological Model Setup

Seven separate geological models were devised using the depth models in section 3.1 – 3.3 (Table. 2). The models were devised to investigate different scales, cavern design, data quality and salt type on the effect on cavern placement. Parameters for the workflow, such as minimum salt thickness and maximum depth were taken from literature and can be found in table 3. Each geological model in table 2 was ran as a montecarlo simulation for a total of 2500 iterations.

Model/Study	Max Salt Depth (Top Cavern) (m)	Minimum Salt Depth (Top Cavern) (m)	Min Salt thickness (m)	Top Salt Surface	Base Salt Surface	Depth Model	Grid Cell Resolution (m)	Temperature (c)	Overburden Pressure Model	Insoluble Content (%)	Cavern Geometry	Depth Uncertainty (%)	Exclusion Zones	Total Area Km^2
Basin Wide – Fixed Caverns	1700	500	358.5	Top Zechstein (Stochastic)	Base Zechstein (Stochastic)	Basin Wide Salt Depth Model (Section 3.1)	250	Distribution, see Appendix (Stochastic)	Gradient – 0.02354 MPa/m (2400kg/m3 equivalent) (Deterministic)	Distribution, see Appendix (Stochastic)	Height: 300 Diameter: 58	10	None	58,904
Sub-Regional - Fixed Caverns	1700	500	358.5	Top Zechstein (Stochastic)	Base Zechstein (Stochastic)	Sub Regional Salt Depth Model (Section 3.2)	50	Distribution, see Appendix (Stochastic)	Gradient – 0.02354 MPa/m (2400kg/m3 equivalent) (Deterministic, but linked to depth uncertainty)	Distribution, see Appendix (Stochastic)	Height: 300 Diameter: 58	5	None	25,000
Layered Evaporite – Variable Caverns	1700	500	200	Top Stassfurt Halite (Stochastic)	Base Stassfurt Halite (Stochastic)	Layered Evaporite Salt Depth Model (Section 3.3.2)	50	Distribution, see Appendix (Stochastic)	Layer cake model (Stochastic)	Distribution, see Appendix (Stochastic)	Variable, Set from height-to-diameter ratio, See Appendix . Maximum height 750 m	7	Interpreted heterogeneity in seismic, Faults (250 m buffer)	238.5
Layered Evaporite – Fixed Caverns	1700	500	358.5	Top Stassfurt Halite (Stochastic)	Base Stassfurt Halite (Stochastic)	Layered Evaporite Salt Depth Model (Section 3.3.2)	50	Distribution, see Appendix (Stochastic)	Layer cake model (Stochastic)	Distribution, see Appendix (Stochastic)	Height: 300 Diameter: 58	7	Interpreted heterogeneity in seismic, Faults (250 m buffer)	238.5
Layered Evaporite - Basin Wide Data - Variable Caverns	1700	500	200	Top Zechstein (Stochastic)	Base Zechstein (Stochastic)	Layered Evaporite Salt Depth Model (Section 3.3.2)	50	Distribution, see Appendix (Stochastic)	Layer cake model (Stochastic)	Distribution, see Appendix (Stochastic)	Variable, Set from height-to-diameter ratio, See Appendix. Maximum height 750 m	10	Interpreted heterogeneity in seismic, Faults (250 m buffer)	238.5
Salt Wall – Variable Caverns	1700	500	200	Top Zechstein (Stochastic)	Base Zechstein (Stochastic)	Sub Regional Salt Depth Model (Section 3.2, cut for Salt – Wall Block)	50	Distribution, see Appendix (Stochastic)	Gradient – 0.2305 MPa/m (2040kg/m3 equivalent) (Deterministic, but linked to depth uncertainty)	Distribution, see Appendix (Stochastic)	Variable, Set from height-to-diameter ratio, See Appendix. Maximum height 750 m	5	500m buffer away from salt wall edges	420
Salt Wall – Fixed Caverns	1700	500	358.5	Top Zechstein (Stochastic)	Base Zechstein (Stochastic)	Sub Regional Salt Depth Model (Section 3.2, cut for Salt Wall -Block)	50	Distribution, see Appendix (Stochastic)	Gradient – 0.2305 MPa/m (2040kg/m3 equivalent) (Deterministic, but linked to depth uncertainty)	Distribution, see Appendix (Stochastic)	Height: 300 Diameter: 58	5	500m buffer away from salt wall edges	420

Table 2: Geological models run through proposed workflow with identified geological parametrisations.

Parameter	Value
Depth to target salt	500 – 2000 m (Warren, 2006, Caglayan et al., 2020, Tan et al., 2021)
Target salt thickness	>200m (Smith et al., 2005, Wang et al., 2015, Caglayan et al., 2020).
Structural heterogeneities	Mapped parameter, buffer set at 250m (Yang et al., 2013, Chen et al., 2022)
Height – to – diameter ratio	0.5 minimum (Wang et al., 2015, Caglayan et al., 2020) Typical no greater than 7.5
Fixed Cavern Size	300 m tall 58.5 m Diameter
Variable Cavern Size	Maximum Cavern Height: 750 m Minimum cavern height: 91.5 m (based on minimum salt thickness 200 m) Maximum height-to-diameter ratio: 7.5 Minimum height-to-diameter ratio: 0.8
Target salt Solubility	No value requirements, needed for hydrogen capacity calculation. Ideally as high as possible.
Energy system integration	Mapped parameter

Table 3. – Salt cavern parameters used within workflow. These parameters are not basin specific and have been gathered from literature on salt cavern development.

4.0 Results

4.1 Basin Wide

4.1.1 Basin Wide – Fixed caverns

The p50 cumulative storage capacity from the basin wide geological model contains is 61.9 PWh (Figure. 6). The p90 and p10 capacities are 49.4 and 80.9 PWh. For cavern number the p50 value is 199,692, with a p90 and p10 of 163,789 and 255,467. The average cavern capacity for the Montecarlo iteration closest to the p50 value (iteration 149) is 308.5 GWh. Iteration 149 of the Montecarlo (geospatial representative of the p50 capacity) can be seen in Figure 6. Individual cavern capacity falls towards the edges of the basin and placement in the basin depocenter is typically restricted to salt structures (Figure 6).

Figure. 6

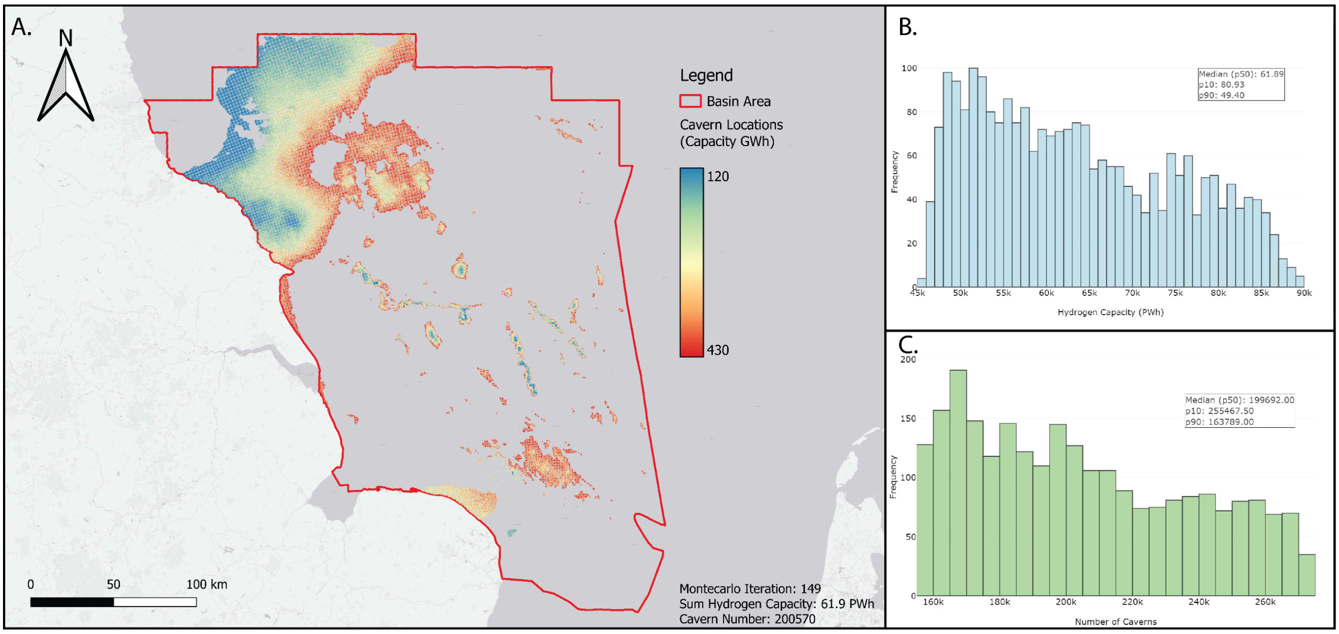

Figure 6 – A) Salt cavern placement map for the 'Basin Wide' AoI with fixed cavern geometries. Geospatial placement represents the output model from the workflow with the closest total hydrogen capacity to the calculated p50 (Iteration 149/2500). A total of 200570 caverns are placed, with a sum of >61.9 PWh of hydrogen storage capacity. B) Histogram of total hydrogen capacities for each iteration of the Montecarlo simulation (2500 iterations). C) Histogram of total cavern number for each iteration of the Montecarlo simulation (2500 iterations).

4.2 Sub-Regional

4.2.1 Sub-Regional – Fixed caverns

The p50 capacity of the sub-regional basin scale geological model is 12.1 PWh, the p90 and p10 are 10.1 and 15.82 PWh's. The cavern number p50 is 36,331 viable cavern locations and the p90 and p10 are 30,233 and 46,674 caverns respectively. Iteration 141 of the Montecarlo simulation is the spatial representative of the p50 result is present in Figure. 7. The locations identified for the development of caverns predominantly show that cavern placement in the mid basin follows the orientation of the major salt structures. 29.7% of caverns of the p50 model are plotted in salt walls and diapirs, despite walls and diapirs only accounting for 5.6% of the total area of the sub-regional basin area (1400 km^2). The remaining 70.3 % of caverns are plotted at the basin edges to the west to north towards the Mid-North sea high, where the cavern placement is more uniformly located in layered evaporite area salt areas (Figure. 7).

Figure. 7

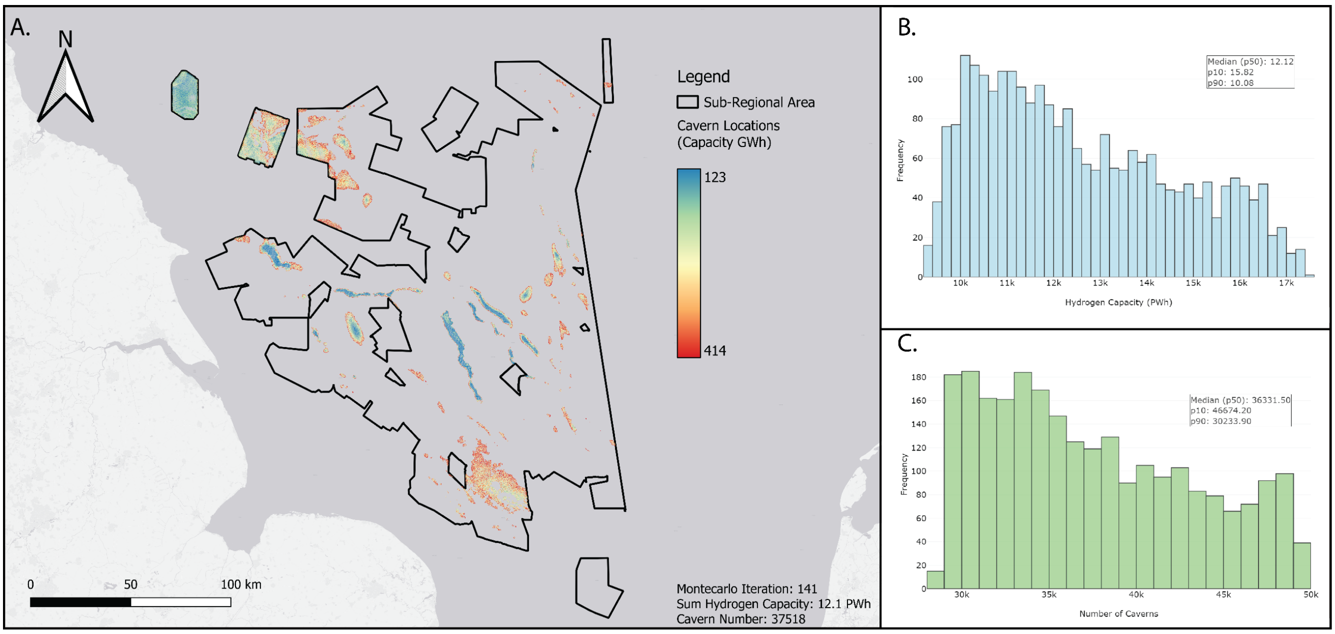

Figure 7 – A) Salt cavern placement map for the 'Sub-regional' AoI with fixed cavern geometries. Geospatial placement represents the output model from the workflow with the closest total hydrogen capacity to the calculated p50 (Iteration 141/2500). A total of 37,518 caverns are placed, with a sum of 12.1 PWh of hydrogen storage capacity. B) Histogram of total hydrogen capacities for each iteration of the Montecarlo simulation (2500 iterations). C) Histogram of total cavern number for each iteration of the Montecarlo simulation (2500 iterations).

4.3 Block Specific

4.3.1 Salt Wall

4.3.1.1 Salt Wall - Variable Cavern

The p50 capacity of the salt wall – variable cavern run is 731 TWh, p90 and p10 capacities are 709 and 752 respectively (Figure 8). We identify 409 caverns could be fit in the salt wall (Figure 8A). Despite the stochastic approach applied to the salt surfaces to account for depth uncertainty, the interpreted salt thickness which is typically greater than 2500 m means that the 5% depth uncertainty does not affect how many caverns can be placed. All caverns had the same geometries despite being set to variable in the workflow. This occurred as all locations had greater thickness than the maximum allowable cavern height (750 m, Table 2-3) and hence had the same height-to-diameter ratio applied to them. This resulted in all caverns volumes before being adjusted for insoluble content to be the same at 5,628,686 m^3.

Figure. 8

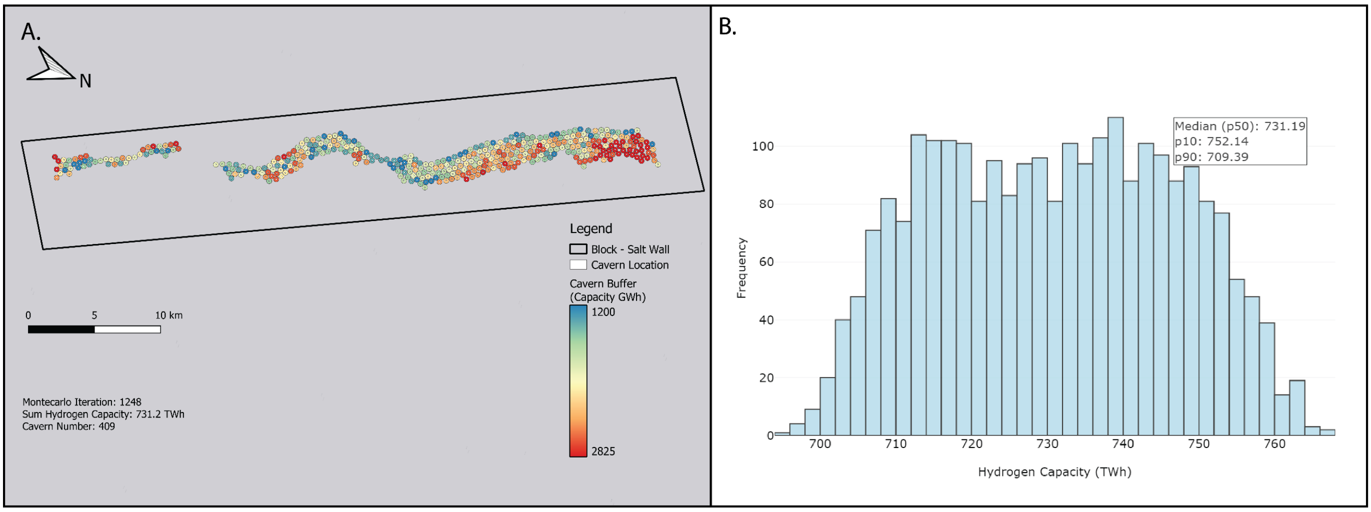

Figure 8 – A) Salt cavern placement map for the 'Block Specific – Salt Wall' AoI with variable cavern geometries. Geospatial placement represents the output model from the workflow with the closest total hydrogen capacity to the calculated p50 (Iteration 1248/2500). A total of 409 caverns are placed, with a sum of 731.2 TWh of hydrogen storage capacity. B) Histogram of total hydrogen capacities for each iteration of the Montecarlo simulation (2500 iterations).

4.3.1.2 Salt Wall - Fixed Cavern

The p50 capacity of the salt wall geological model with caverns of fixed geometry (Table. 2-3) was 225 TWh, the p90 and p10 results are 219 and 231 TWh (Figure. 9). The total number of viable cavern locations within the area ranges between 1154 and 1151, depending on the depth uncertainty applied (Figure. 9). Small edge case variations between the Montecarlo iterations caused by the associated depth uncertainty %, cause small areas to become viable and nonviable, causing the small change in cavern number, similar to that of the salt wall variable cavern number.

Figure. 9

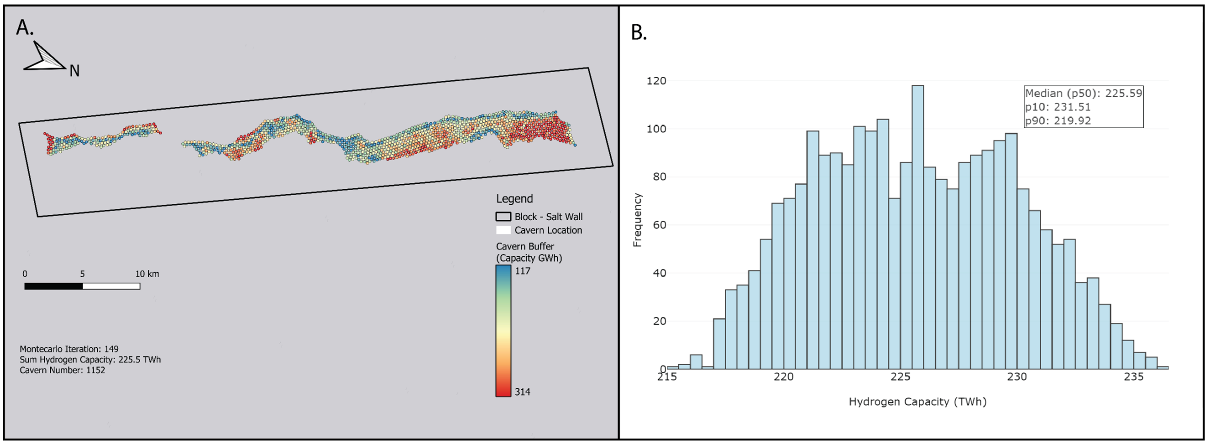

Figure 9 – A) Salt cavern placement map for the 'Block Specific – Salt Wall' AoI with fixed cavern geometries. Geospatial placement represents the output model from the workflow with the closest total hydrogen capacity to the calculated p50 (Iteration 149/2500). A total of 1152 caverns are placed, with a sum of 225.5 TWh of hydrogen storage capacity. B) Histogram of total hydrogen capacities for each iteration of the Montecarlo simulation (2500 iterations).

4.3.2 Layered Evaporite

4.3.2.1 Layered Evaporite - Variable Cavern

The p50 capacity of the layered evaporite – variable caverns geological model is 419.2 TWh, p90 and p10 are 387.5 and 449.5 TWh. The p50 for cavern number is 448 viable cavern locations (Figure. 10, Table. 4) with 358 and 501 for the p90 and p10 cavern locations respectively (Figure. 10, Table. 4). Table 4 has the closest model iterations output to the p10, p50 and p90 capacity values (Figure 10). The iteration closest to the p50 has the smallest number of caverns present (as our workflow optimises for capacity), however it has the largest working average cavern working capacity with 2330 GWh compared with 2079 GWh of the p90 and 2004 GWh of the p10. Whilst the model closest to the p10 has the lowest average working capacity per cavern, it has the greatest total working capacity, this is due to the increased number of caverns present in this model iteration compared with the other models. The iterations closest to the p50 and p90 have a similar number of caverns placed, however the p50's greater average working capacity gives the model greater total working capacity.

Outcome	Total Working hydrogen Capacity (TWh)	Total Cavern Number	Average Cavern Working Capacity (GWh)	Smallest Cavern Working Capacity (GWh)	Largest Cavern Working Capacity (GWh)	Energy Density (TWh/Km^2)
P90 (Iteration: 1590)	387.5	337	1149.9	309.7	2215.1	1.72
P50 (Iteration: 175)	419.2	467	897.6	259.5	1990.2	1.86
P10 (Iteration: 1128)	449.5	478	940.4	255.3	1991.8	2.00

Table 4 – Results of Montecarlo simulation, iterations closest to P values from Layered evaporite – Variable cavern geometries

Figure. 10

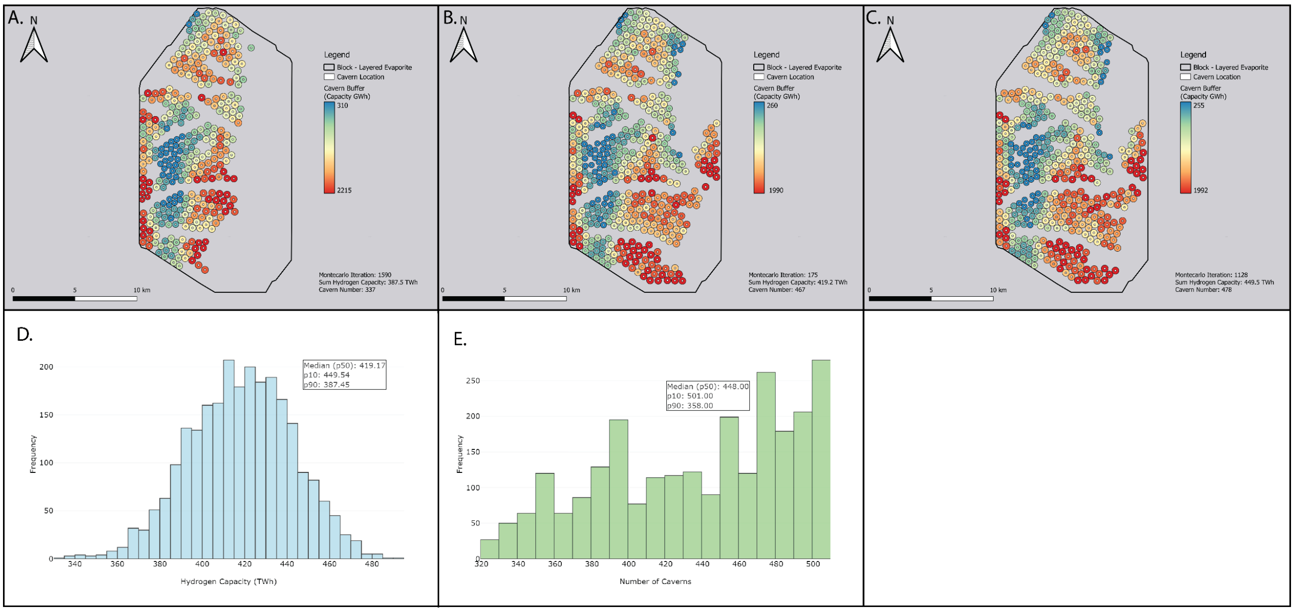

Figure 10 – Salt cavern placement maps for the 'Block Specific – Layered Evaporite' AoI with variable cavern geometries. Geospatial placement represents the output model from the workflow with the closest total hydrogen capacity to the calculated p90 (A, Iteration: 1590),

p50(B, Iteration: 175), and p10 (C, Iteration: 1128). D) Histogram of total hydrogen capacities for each iteration of the Montecarlo simulation (2500 iterations). E) Histogram of total cavern number for each iteration of the Montecarlo simulation (2500 iterations).

4.3.2.2 Layered Evaporite - Fixed Cavern

The p50 capacity of the layered evaporite – fixed caverns geological model is 260.3 TWh, 158.9 TWh less than that of the variable cavern model for same AoI (Figure. 11). The p90 and p10 capacity values are 184.8 and 277.6 TWh respectively. The p50 for cavern placement is 832, p90 and p10 for cavern number are 606 and 861 viable locations. The iteration from the Montecarlo simulation with the closet hydrogen value to the p50 capacity has a total of 839 viable cavern locations, 372 more caverns than the equivalent variable cavern p50 iteration. The fixed caverns however have a much lower average capacity, with value of 310 GWh, compared with 1990 GWh of the variable caverns.

Figure. 11

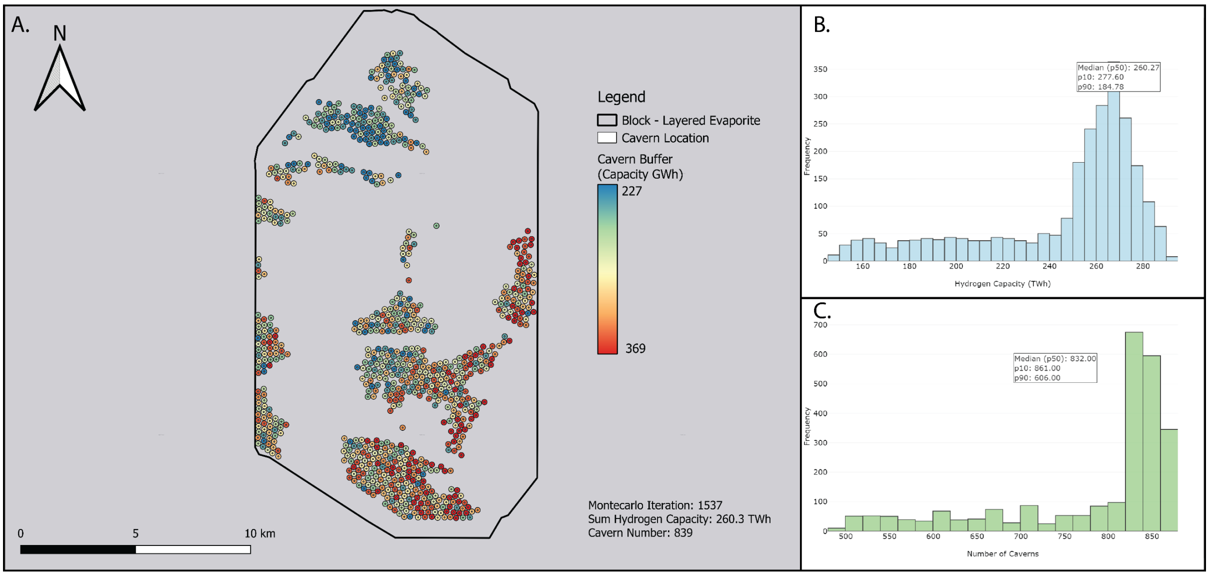

Figure 11 – A) Salt cavern placement map for the 'Block Specific – Layered Evaporite' AoI with fixed geometries. Geospatial placement represents the output model from the workflow with

the closest total hydrogen capacity to the calculated p50 (Iteration 1537/2500). A total of 839 caverns are placed, with a sum of 260.3 TWh of hydrogen storage capacity. B) Histogram of total hydrogen capacities for each iteration of the Montecarlo simulation (2500 iterations). C) Histogram of total cavern number for each iteration of the Montecarlo simulation (2500 iterations).

4.3.2.3 Layered Evaporite - Basin Wide Depth Model – Variable Cavern

The p50 capacity of the layered evaporite – basin wide depth model - variable caverns was 798.7 TWh (Figure. 12), the p90 and p10 capacities are 727.1 and 889.5 TWh. The p50 for cavern placement is 495, p90 and p10 for cavern number are 479 and 503 viable locations. The resultant geospatial distribution of the caverns differs from the site-specific depth model (4.4.1), as there are large gaps between placed caverns (Figure. 12). The caverns placed have a higher average capacity than the site-specific geological model (Section 4.4.1) 1616.7 GWh vs 897.6 (closest iteration to the p50 capacity of both models).

Figure. 12

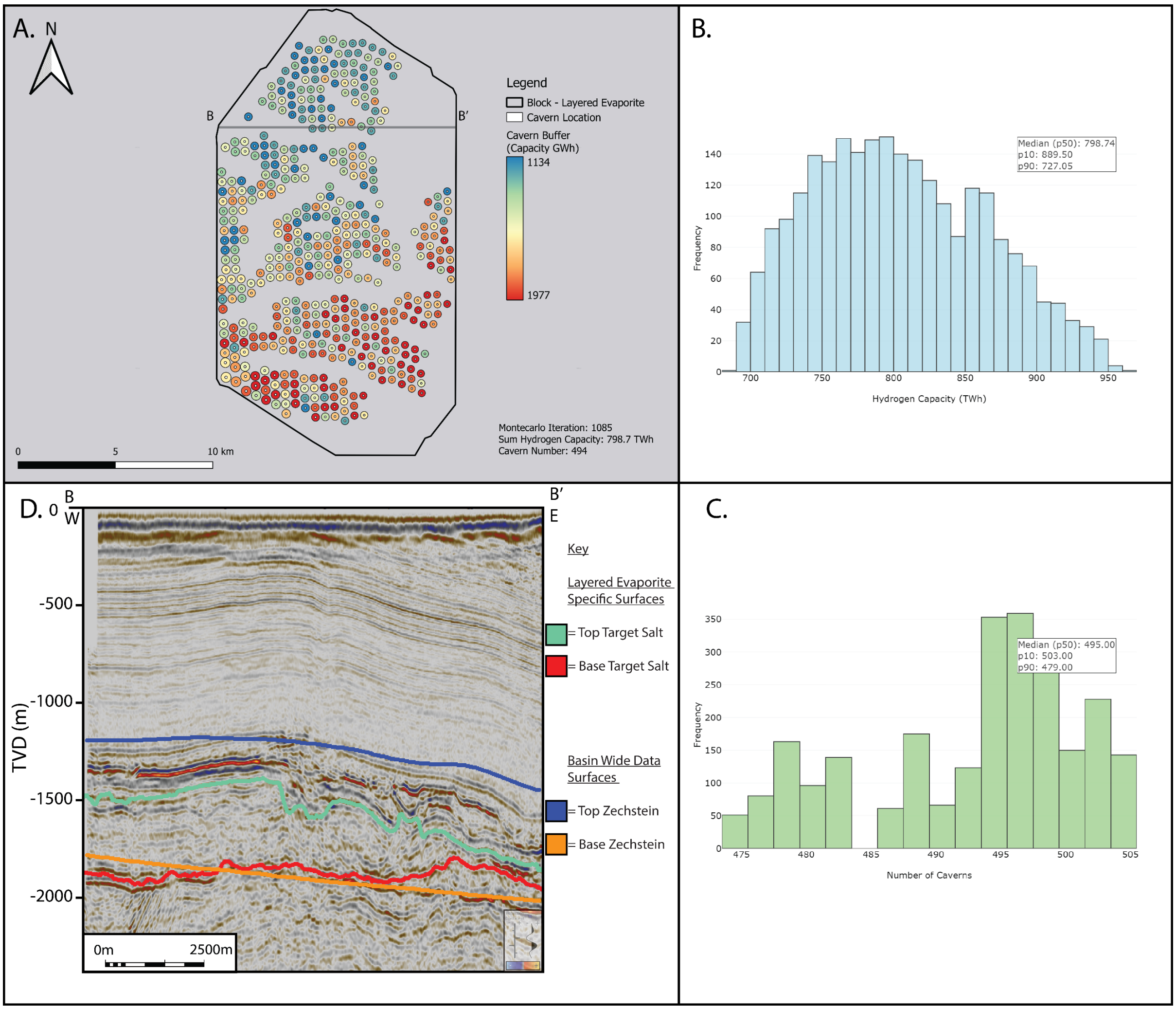

Figure 12 – A) Salt cavern placement map for the 'Block Specific – Layered Evaporite' AoI with variable cavern geometries and using the Basin Wide AoI depth surfaces. Geospatial placement represents the output model from the workflow with the closest total hydrogen capacity to the calculated p50 (Iteration 1085/2500). A total of 494 caverns are placed, with a sum of 798.7 TWh of hydrogen storage capacity. B) Histogram of total hydrogen capacities for each iteration of the Montecarlo simulation (2500 iterations). C) Histogram of total cavern number for each iteration of the Montecarlo simulation (2500 iterations). D) Seismic cross section running West to East, B – B' (Figure. 4,12), in TVD (m). Stassfurt halite surfaces interpreted from seismic survey MA933F002 and depth converted are present, Green (Top Stassfurt Halite) and Red (Base Stassfurt halite / Top basal polyhalite). Blue and orange lines

represent publicly available depth surfaces acquired from the NSTA of the top and base Zechstein, used for the 'Basin Wide' AoI geological model.

4.4 Conceptual cavern cluster developments

While cumulative hydrogen capacity across large tracts of basins may be useful for initial comparison of storage potential, a more useful consideration is the capacity of a salt cavern cluster development. We therefore consider five conceptual salt cavern cluster developments as a demonstration of how the workflow could aid in early-stage planning for a possible cavern site at the project pre-feasibility stage (Figure. 13). The theoretical cluster concepts were developed using iteration 175 (Figure. 10) from the Montecarlo simulation, the iteration where the sum hydrogen capacity was closest to the p50 of the block specific – layered evaporite – variable cavern model (Section 4.4.1). We assume three different development scenarios 1) Maximum hydrogen storage capacity within a 1.5 km radius of fixed point; 2) Maximum hydrogen storage capacity within a 3 km cluster radius of fixed point; 3) Maximum cavern number within a 1.5 km radius of fixed point; 4) Maximum cavern number within a 3km radius of fixed point; 5) Storage capacity within 1.5 km radius of pre-existing infrastructure (wellbore 41/05-1) (Figure. 2). Radiuses of 1.5 – 3 km are considered viable step-out or deviation distances from a central facility point for development of individual caverns. The geographic layout of the development concepts is shown in Figure. 13, and a summary of results is in Table. 5.

Figure. 13

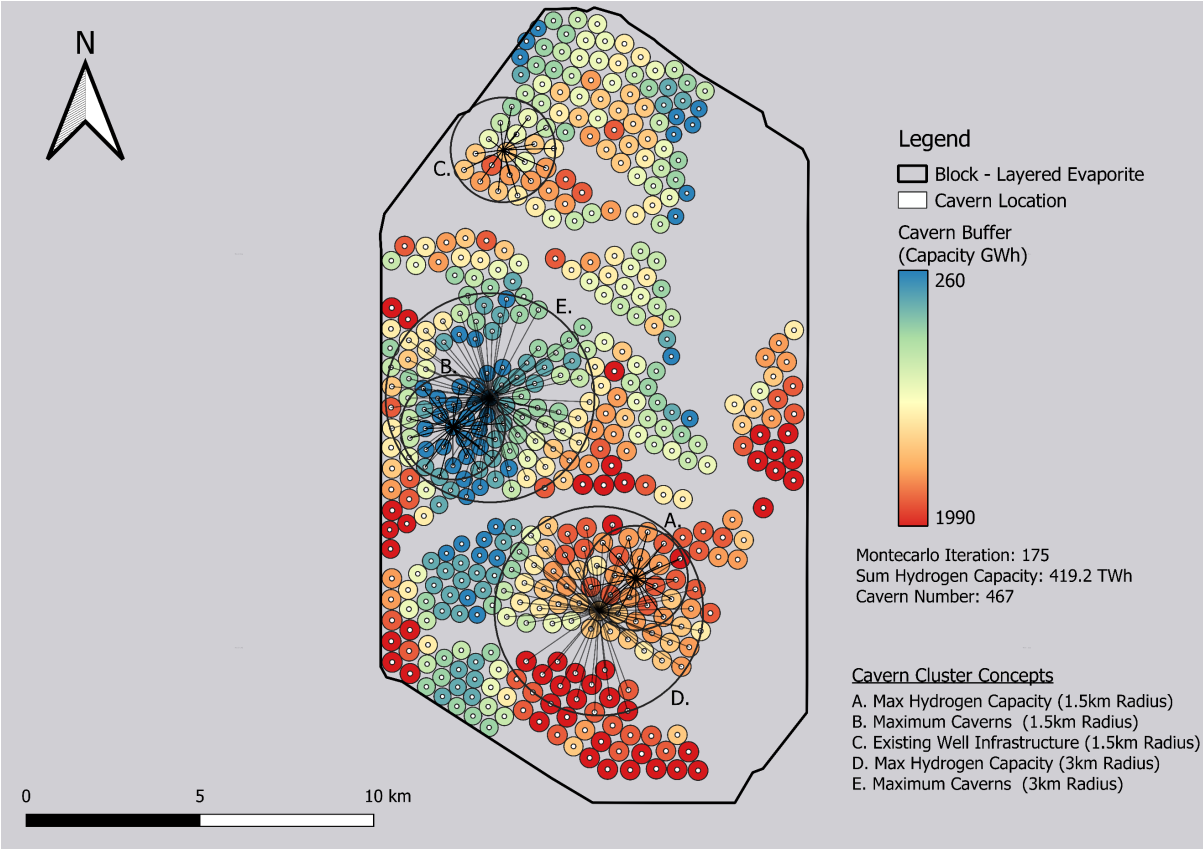

Figure 13 - Salt cavern cluster concept play map. Base salt cavern map is the representative p50 of the 'Block - Layered Evaporite' AoI variable cavern model (Figure. 10 B). 5 possible cavern cluster concepts are described A) Max hydrogen capacity within a 1.5 km radius. B) Maximum cavern number within a 1.5 km radius. C) 1.5km radius placed upon existing infrastructure (wellbore 41/05-1, Figures. 2, 5). D) Max hydrogen capacity within a 3 km radius. E) Maximum cavern number within a 3 km radius. Radiuses were chosen as such to mimic offshore infrastructure.

Cluster	Total Hydrogen Capacity (TWh)	Cavern Number	Pipeline / Deviation length (km)
A – Max Hydrogen Capacity 1.5km radius	26.9	22	22.3
B – Maximum Caverns (1.5km radius)	10.2	28	28.5
C – On existing well	18.7	19	18.4
D – Max Hydrogen Capacity (3 km radius)	84.4	72	141.5
E – B – Maximum Caverns (3km radius)	51.2	91	181.6

Table 5. Theoretical salt cavern cluster information (Figure. 13)

5. Discussion

5.1 Capacities and volumetrics and cavern placement

The results described demonstrate the value in stochastic approaches to evaluating geological energy storage. The case studies demonstrate the importance of high veracity geological models as inputs for such analysis. The results presented indicate that theoretically salt cavern capacity offshore could meet all existing scenarios for the UK's required hydrogen storage, 40 – 115 TWh as suggested by Electricity System Operator (2023) and Cárdenas et al. (2021).

The basin wide and sub-regional investigations demonstrate there are up to 10's of PWh of potential storage within the Southern North Sea for hydrogen (Figures. 6-7), an order of magnitude greater than is required, and several times larger than the estimate working capacity of depleted gas fields and aquifers in the same location (2661 TWh) (Jahanbakhsh et al., 2024). The p50 of possible cavern locations estimated is 199,692 (Basin Wide geological model) and 36,331 (Sub-Regional geological model), clearly providing extensive possible sites for consideration for development in the future. When the total number of caverns is so high, the total capacity across is largely irrelevant. Value from our Basin wide and Sub-Regional results hence does not come from the capacity of hydrogen storage, but rather the cavern number and placement, both factors being required for energy systems planning (Samsatli and Samsatli, 2019). At a block scale the results from using higher resolution geological models (Figures 8 – 13) demonstrate that areas equivalent to individual licence areas (average 115 km^2, largest 250 km^2) the number of feasible cavern locations, and the total capacity are far greater than current scenarios for the UK's required hydrogen storage (Cárdenas et al., 2021, Electricity System Operator, 2023).

By considering clusters of caverns (e.g. Figure. 13) we make use of the spatial outputs of the model to compare the merits of different cluster development locations. We examine conceptual salt cavern cluster developments in the layered evaporite area, using the variable cavern montecarlo iteration closest to the p50 capacity value (Figure 10, 13) as the base case. The development concepts, although lacking integral detailed engineering constraints built in, are limited to spatial extents that are feasible with existing technologies (Energy Technologies Institute, 2013). The principal consideration is the step out distance from a fixed offshore infrastructure point, for which we have considered distances of 1.5km and 3km. The distance from the fixed centre point to the centre of each theoretical cavern location is considered a viable representation of either a) a seabed pipeline distance to tie back individual caverns, or b) the drilling of a deviated well with a step out. The examples shown are to demonstrate the value of the outputs from the workflow we have developed. Both cavern cluster concepts, E and D, had sufficient capacity to match the minimum required energy storage set by Cárdenas et al. (2021), however these both still had very large number of caverns present >50. Cluster A, however, with 26.9 TWh potential is close to the 42 TWh requirement, with only 22 caverns and 22.3km of pipeline, a typical salt cavern cluster development consists of up to 35 caverns (Gillhaus, 2007).

5.2 Comparison to other studies

Previous studies have evaluated the offshore storage capacities for salt caverns in the Southern North Sea. We compare our results to these (Table. 6). Previous studies suggest there is also greater than required energy storage capacity within the both the onshore and offshore salt basins domains.

The results of our study are in line with Caglayan et al. (2020) indicating there are PWh's of potential storage within the offshore of the UK in the Southern North Sea. Caglayan et al. (2020) only places cavern locations within 47 salt structures within the Southern North Sea, whereas our salt structure maps have 42 unique structures within our sub-regional depth model, which may account for the differences. These values suggest the Southern North Sea's capacity for LDES in salt caverns far exceeds any onshore basin within the UK (Table. 6)

Whilst basin wide capacity may be useful to benchmark one basin against another, all the estimates demonstrate that the total of all possible cavern locations far exceeds the UK storage requirements (Table. 5). For geographic areas with laterally extensive salt, the issues that are most pertinent are not related to total capacity, but rather to identifying the optimum geographic location of development clusters relative to other infrastructure. Our workflow allows for this geospatial investigation. This has implications for the development of energy production infrastructure, such as industrial clusters, marine renewable infrastructure and hydrogen production facilities, because the proximity of energy storage, production and usage are important factors in considering whether sites next to each other can be advantageous (Walsh et al., 2023). It can also aid with dictating the ease of development for the caverns, for example, how many caverns can be emplaced in a suitable shallow offshore setting or within a set buffer distance of previously mentioned infrastructure.

Study	Basin/Area	Working Hydorgen Capacity (TWh)	Number of Caverns	Average Cavern Working Capacity (GWh)	Cavern dimensions
Williams et al. (2022)	Cheshire Basin	129	1297	99.4	Height: 20 -262 Diameter: 100 m
Williams et al. (2022)	Wessex Basin	557	3378	164.8	Height: Variable Diameter: 100 m
Williams et al. (2022)	East Yorkshire	1465	8425	173.9	Height: Variable Diameter: 100 m
The Royal Society (2023)	East Yorkshire	≈100	3000	33.3 (Estimates of 120 in chosen locations)	Height 100m Diameter 31m Raw Volume: 300,000
Caglayan et al. (2020)	Offshore UK (Southern North Sea, Salt structures only)	9,000	NA	NA	Height 300 Diameter 58 Raw Volume: 750,000
*Basin Wide – Fixed Caverns – p50 (Iteration: 149)	Offshore UK (Southern North Sea, 58,904 km^2)	61,885	200,570	308.5	Height 300 Diameter 58 Raw Volume: 750,000
Allsop et al. (2023)	Offshore UK – (Mega Merge Area - Southern North Sea)	53 - 292	1485	35.6 / 196.6	Height 300 Diameter 58 Raw Volume 750,000
*Sub-Regional – Fixed Caverns – p50 (Iteration: 141)	Offshore UK – (Mega Merge Area – Southern North Sea, 25,000 km^2)	12,124	37,518	323	Height 300 Diameter 58 Raw Volume: 750,000
Allsop et al. (2023)	Audrey Salt Wall	23 - 105	105	219 / 1005	Height 300 Diameter 58 Raw Volume: 750,000
*Salt Wall - Fixed Caverns - p50 (Iteration: 149)	Audrey Salt Wall	225	1152	195	Height 300 Diameter 58 Raw Volume: 750,000
*Salt Wall – Variable Caverns - p50 (Iteration: 1248)	Audrey Salt Wall	731	409	1787	Variable
*Layered Evaporite - Variable Caverns - p50 (Iteration: 175)	Seismic Survey - MA933F002	419	467	897	Variable
*Layered Evaporite – Basin Wide Depth Model Data - Variable Caverns p50 (Iteration: 1085)	Seismic Survey - MA933F002	799	494	1617	Variable
*Layered Evaporite – Fixed Caverns p50 (Iteration: 1537)	Seismic Survey - MA933F002	260	839	309	Height 300 Diameter 58 Raw Volume: 750,000

Table 6. Note results from this study regarding cavern number are obtained from the Montecarlo iteration (Iteration number in brackets, see data for Montecarlo iteration list) with the closest total hydrogen capacity to the calculated p50 for that model run. * = models from this study.

5.2 Limitations of workflow/approach

As with any subsurface modelling method, there are limitations. We use variable cavern geometries, and frequently the capacities these are calculated to have volumes greater than those frequently stated in literature (Table 6.). These volumes do not exceed the volume of the largest documented cavern, which has a total volume of 17,000,000 m^3 (670 m tall and 180 m diameter) (Leith, 2000). We compare the results of modifying cavern geometries while keeping every other parameter the same as seen in Table. 6 (Layered evaporites – Variable Caverns - p50 vs layered evaporite – Fixed Caverns - p50 Models). Allowing for larger and variable cavern geometries allows for higher storage capacities within an area. However, there are fewer caverns placed within these runs (Table. 6), if the placement of caverns was of important consideration, smaller caverns may be favoured as they allow for greater opportunities in their placement. Fewer, larger caverns would allow for less drilling in the development of a possible cluster, allowing the initial capex of a site to be reduced.

While our geological models capture the thickness changes and the 3D structures of the Zechstein of the Southern North Sea, they did not incorporate the internal 3D heterogeneities that may be present. For the layered evaporite area, however, we chose to take a 2D approach by mapping areas of none-viability such as faults and generalised areas of insolubility and removing them as deterministic nonviable areas. However, within the salt structures, none-soluble stringers and complex geometries are typically associated with the internal structural heterogeneity (Pichat, 2022). Imaging in salt structures is typically poor both due to the complex ray paths in the crystalline structure of salt, and seismic surveys often being designed to image post and pre-salt (Jones and Davison, 2014). As such the 3D heterogeneity for the salt structures investigated was not incorporated within the workflow. Further work could be undertaken, such as in (Teixeira et al., 2020), utilizing quantitative interpretation of the seismic data to identify areas of low solubility and incorporate them into the workflow.

Evaporite units are known to cause thermal anomalies in heat distributions within the subsurface, due to their crystalline structure conducting heat energy more efficiently than the surrounding lithologies (Jackson and Hudec, 2017). The increased complexity of 3D heat flow makes using a geothermal gradient inappropriate for salt, with a 1D thermal or 3D heat cube being more suitable. These approaches were outside the scope our work unfortunately. However, with the flexibility of our workflow, had thermal modelling been within the scope of this study, or been available to utilise later, it would have been straightforward to incorporate this dataset within our workflow.

The geomechanics of cavern emplacement were not considered in detail within our workflow. The distances used for geomechanical stability between caverns was taken from literature and determined as suitable for our workflow development (Allen et al., 1982, Caglayan et al., 2020). Area specific geomechanics models could be incorporated into our workflow for more suitable cavern placement, but the development of such was outside the scope of our research.

Despite these limitations observed in our own usage of our workflow, it has been designed in such a way that it is easily modified for different geological models, parameters, or uncertainties. This is seen by the number of different cases and iterations we have run, where the inputs to the workflow have been modified to be more suitable with the input geological model.

5.3 Veracity of data

The necessity for geological models to be reliable and reproducible is essential where they underpin vital developments as part of sustainable pathways and in achieving Net Zero (Steventon et al., 2022). We compare the layered evaporite salt model using seismic specific data (Sections 4.1.1, Figure 10) and using basin wide depth data (Section 4.1.3, Figure 12). Both models use the same parameters with only the surfaces and associated depth uncertainty changing (Appendix. 2). The changing of surfaces causes a number of items to be affected: 1) the formation thickness changes because the basin wide data is from top to base Zechstein, whereas the site-specific surfaces are from top to base Stassfurt halite (Figure 5). 2) The depth to the top salt is different, with the basin wide model being shallower, allowing for more viable locations. 3) The grid cell resolution is also different; Appendix. 2 shows the differences in surfaces. The basin wide data results estimate 27 more caverns, 380 TWh higher capacity, and an average cavern working capacity of 720 GWh higher than the specific data geological model. These differences arise from the basin wide data use of the top and base Zechstein as input, rather than having the specified salt target, which in turn causes the salt to be thicker, allowing for larger caverns to be placed by the workflow. Using the top and base Zechstein also causes non-soluble stratigraphic layers within the Zechstein, such as the Plattendolomit (Figure. 3,5), to be within the area for cavern emplacement in the workflow. If a stratigraphic layer, such as the Plattendolomit, were to be encountered while attempting to solution mine a cavern it may cause many issues, such as cavern collapse, inability to continue solution mining, contamination, or act as a porous and permeable pathway for hydrogen to escape, and, as such should be avoided (Chen et al., 2018, Zhang et al., 2021, Zhu et al., 2023).

The public surfaces are also lower resolution with a grid cell spacing of 250 m, as opposed to 50m. This lower resolution leads to ineffective packing of the caverns (Figure 12A), as the grid cell size is greater than the typical buffer (~100 m) between adjacent caverns. A higher resolution model enables not only more potential cavern locations to be considered, but also captures a higher resolution of structural variability in the geometry of the salt interval. The work presented here suggests that the minimum grid cell size of the input geological model is at most 4x the minimum cavern size diameter, as this will allow for every grid cell to have a point with minimum overlap. If the resolution was any lower, the circles would be inefficiently packed. It is advised however that grid cell resolution should be higher than this to allow for more caverns than necessary to be generated, as this will lead to better cavern packing (Figure. 14).

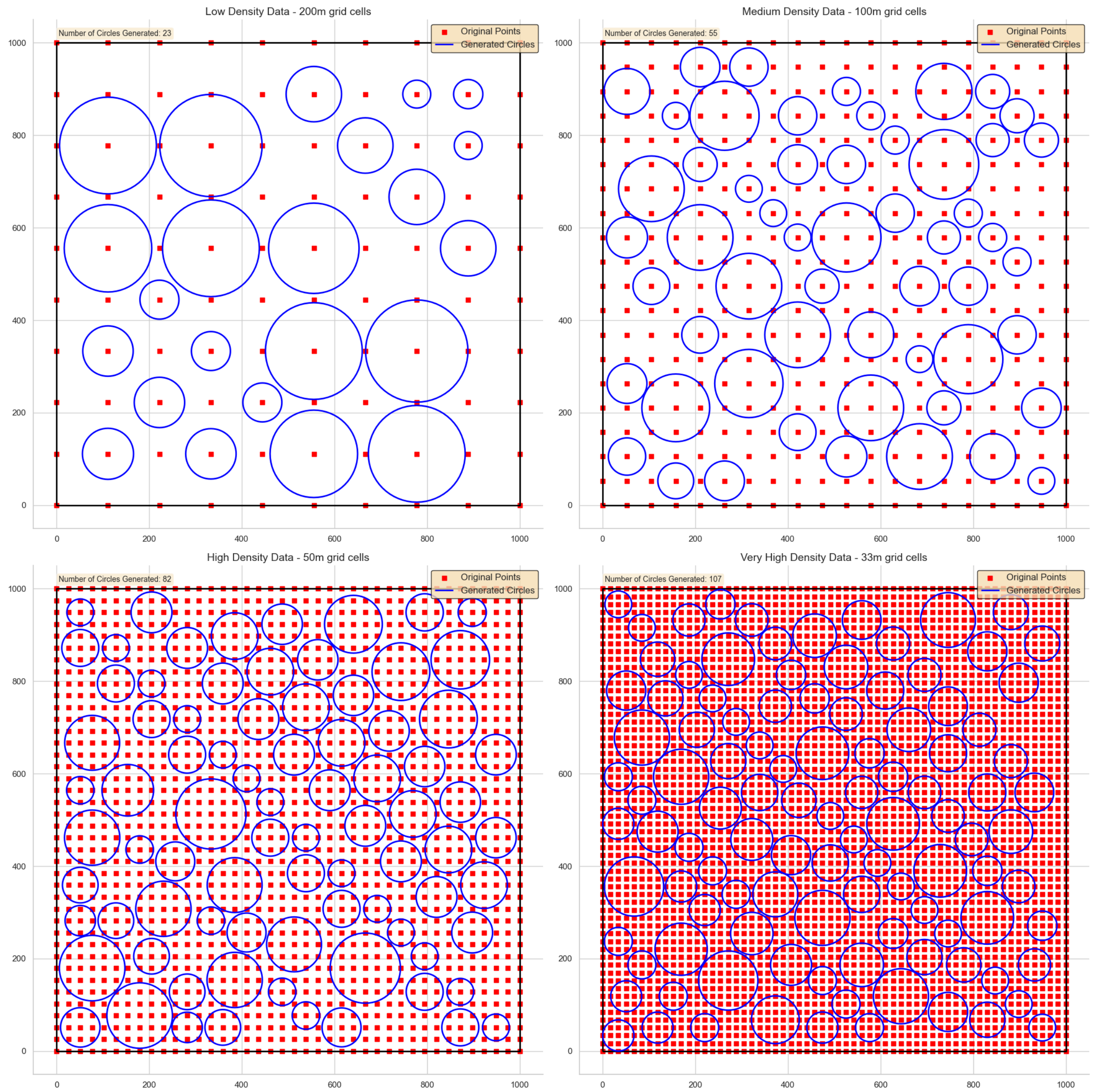

Figure 14 – Synthetic grid data surfaces of varying data density (200 m – 33 m) with circles generated using the same buffer packing function that is used within the cavern placement workflow (Section. 2.1). The different grid densities and generated circles demonstrate how input grid density (geological model grid cell density) affects the location and placement of caverns.

5.4 Importance of reproducibility and replicability

Within subsurface geosciences, practical frameworks for reproducibility are in their infancy, particularly where there are significant uncertainties related to data (Steventon et al., 2022). In particular it has been identified that availability of data and software (including code), frequently limit the possibility of reproducing studies (Ireland et al., 2023). Previous studies into geological energy storage estimates rarely provide sufficient information to be reproduced. This study has made available the code through a CC BY-SA so that it can be used, revised, and modified, including for commercial purposes. This therefore allows others to test the replicability of our method (e.g., same method, different data). As well as the method, it is vital that the underlying data for studies are made available (Hardwicke et al., 2018). Previous studies of geological energy storage do not provide the data used for the capacity estimates, thus limiting the opportunity to examine the reliability of the estimates. In this study we use data, and interpretations from existing open licence sources (NSTA), as well as our own interpretations, which we also make available through CC-Y licence. This approach allows for all our results to be fully reproducible and replicable.

The comparison shown in Table 6 highlights the importance of reproducibility and reliability in studies where results may have implications for both the scientific community and policy makers. The results from Caglayan et al. (2020) and Allsop et al. (2023), for the same areas indicate differences of up to 3124 TWh and 11,832 TWh respectively (compared with sub-regional model). With such large differences in predictions, it is important to be able to understand where such differences arise from, however replicability is only viable when the original data is published. While our capacity calculations are larger than the those proposed in Caglayan et al. (2020), they both agree that there is PWh storage potential of hydrogen within the Southern North Sea, with our sub-regional model differing by 29.5%, while using different subsurface datasets (Caglayan et al. (2020) do not incorporate layered evaporite domains into their geological model). Allsop et al. (2023) estimated significantly different capacities in comparison to this study, for both the salt wall and the sub-regional model (Table 5) while using the same seismic data (2016 Southern North Sea Mega-merge). They estimate that only 1485 caverns can be emplaced within the entirety of sub-regional area, as opposed to 34,108 in our study, and only 105 within the Audrey salt wall as opposed to the 1154 presented here (using the same cavern geometries) (Figure. 7,9). Unfortunately, due to the lack of detail in the methodology and results (no geospatial data regarding cavern placement) presented by Allsop et al (2023) we were unable to make a detailed comparison between each workflow and understand where these differences originated. Allsop et al. (2023). This example of researchers reaching different conclusions while utilising the same dataset emphasises the importance of reproducibility and replicability in geoscience There are many studies in the geoscience community, where the results are unable to be reproduced or replicated (Ireland et al., 2023). When all aspects of research are open this improves their trustworthiness (Rosman et al., 2022), which is essential if findings are to inform policy or aspects of national planning, such as energy systems (UK Government, 2012).

5.5 Energy system integration.

The outputs generated from our workflow are such that they contain individual cavern locations, specification, and capacities. These outputs can be used as inputs into further energy systems modelling that include storage e.g Sunny et al. (2020). Energy system models and energy value chain studies, while having offshore energy generation within their models, typically implement storage opportunities within the onshore domain, not offshore, limiting opportunity and constricting possible energy solutions (Samsatli and Samsatli, 2019). Aiding in the design of energy systems can occur at all scales because of the different geological models that were run through our workflow (broad whole basin geological models to site specific models).

The geographic results, both individual caverns and conceptual clusters can be reviewed with respect to important energy infrastructure. For example, Figure. 15 shows the number of caverns and capacity within 20km radius of existing and planned offshore wind developments in the Southern North Sea. Of the 32 developments, 15 have > 1000 viable cavern locations and 15 have over 500 TWh of viable hydrogen capacity (Figure. 1). We can also examine the setting of cavern locations, such as water depth or distance from the coastline, both which could impact the development cost (Energy Technologies Institute, 2013). All cavern locations are situated in under 100 m water depth, which means all could be developed by a jack-up ship (limits are typically 120m). There are 21,000 possible cavern locations within 10 km and 37,000 within 20 km of the east coast (Basin wide model).

These are some possible examples as to how the output from this study and our workflow could be integrated into energy systems design. While our brief overview of this is simplistic, our data could be used for much more complex analysis because of the level of information associated with each cavern generated.

Figure. 15

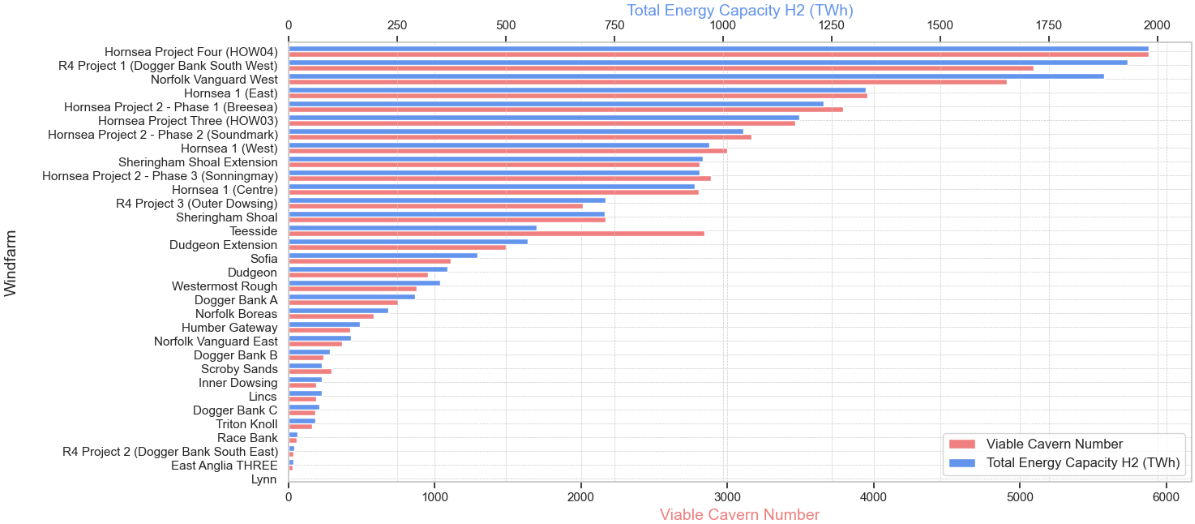

Figure 15 – Windfarms located within the 'Basin Wide' AoI (Figure. 6), plotted against viable cavern number and total hydrogen storage capacity within a 20km buffer of the windfarm site (Basin Wide results used (Section 4.1.1)).

5.6 Offshore salt caverns for LDES

To date, all salt caverns have been emplaced onshore, however offshore salt cavern projects have been proposed before (Evans and Holloway, 2009) (Figure 1). We have demonstrated that not only does the total capacity available exceed current estimates for storage, but that the number of viable geographic locations offshore has the potential to provide effective integration with current and future marine renewable infrastructure (Figures. 6,7,15). The integration of salt cavern clusters for LDES could provide greater flexibility and variability in the generation of energy from offshore renewables (Arellano-Prieto et al., 2022). The idealised location for caverns is next to hydrogen production hubs, those generating either blue or green hydrogen, optimising the integration, flexibility and transport of hydrogen from production to storage (Walsh et al., 2023).

Subsurface/infrastructure work that occurs offshore has costs associated with it that are higher than those that occur onshore, for example wind turbines are 50% more expensive offshore than onshore (Bilgili et al., 2011). Savings might be possible in regard to salt caverns, as disposal of brine produced by the creation of the salt caverns into the sea will be more cost effective than the cost of transporting the brine onshore. The cost of pipelines will need to be a key aspect of site consideration as they will be a significant component of the CAPEX costs. Throughout our theoretical salt cavern sites, we have modelled the possible distances of pipeline for a single cluster to get reasonable estimates as to what may be required, however a more thorough specific investigation into this will be needed.

Alternate energy vectors could be stored within salt caverns to alleviate carbon emissions in other industries. Global shipping accounts for 2% of global carbon dioxide emissions, both ammonia and methanol have been suggested as replacement 0 emission fuel sources (Svanberg et al., 2018, Gallucci, 2021). At the average internal pressure/temperature conditions of the salt caverns from our basin wide study (64 °c and 36.2 MPa), ammonia would be in its super critical phase and methanol would be in its liquid phase (National Institute of Standards and Technology, 2023). Ammonia has previously been suggested as storable within salt caverns (Adams and Cottle, 1954). Combining storage and offshore production of these zero emission fuels would allow for an fully integrated green ship refuelling ecosystem. If salt caverns are unsuitable for these energy vectors for reasons we may have missed, hydrogen stored within the caverns could be used as a feedstock for a surface production facility for these possible fuels.

6. Conclusion

Within this paper we have demonstrated our proposed workflow using several geological models and parameters. We position this workflow at the pre-feasibility stage of an area for the investigation placement of salt caverns. The workflow takes a geological model as an input and outputs valid salt cavern locations alongside capacity estimates. The workflow has been designed that such that any parameter and variables can be changed to suit the geological model and area of interest, even allowing the chosen energy vector to be altered. The workflow allows for the input of not only deterministic values but stochastic values, allowing to compensate for the uncertainty typically associated with geological models of the subsurface.

From our workflow we produce realistic theoretical salt cavern clusters that help to show how the results from our model could be used to develop such a cluster. The capacity results show that a single large offshore cavern cluster (with a 3km diameter AOI) may have enough hydrogen storage capacity to meet the UK's long duration energy storage requirements in full. The workflow and associated data should be used to aid site planners or policy setters to making further decisions regarding hydrogen storage offshore using salt caverns.

The offshore domain is often not considered when deciding where LDES should be placed. We have demonstrated that the offshore of the UK is a suitable location, with over 199,000 locations of caverns and PWh scale capacity for hydrogen. This viability of the offshore domains opens possible co-location with offshore energy production hubs, allowing for the UK to have a full green energy production hub operating offshore.

We also compare our results against other studies to emphasise how important it is to have a reproducible and replicable methodology. All code, data and interpretations used within this study are supplied within the data repository.

Appendix

Appendix 1.

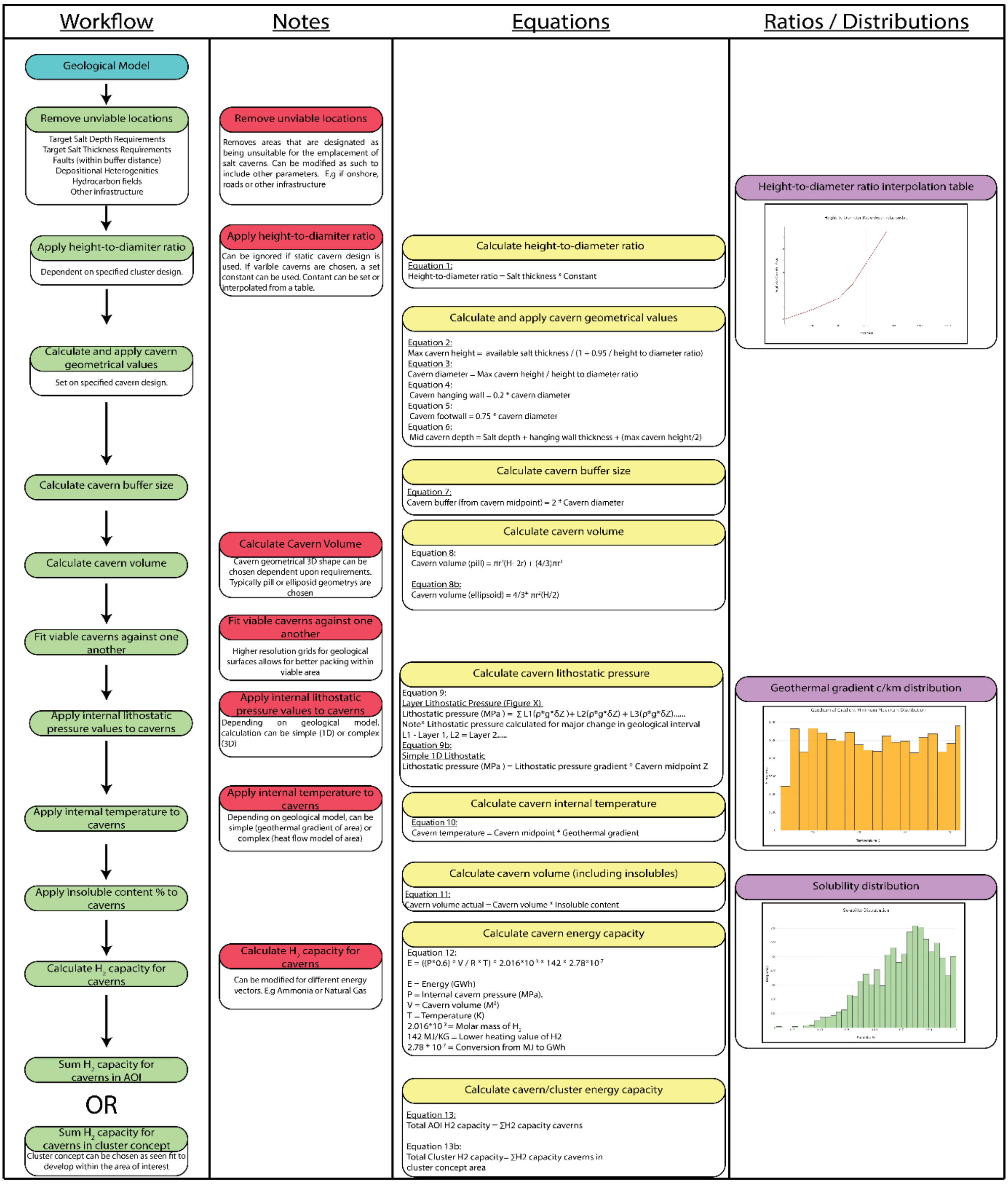

Appendix 1 - Workflow, equations, and ratios/distribution used for the methodology described in Section. 2.

Appendix 2.

Appendix 2

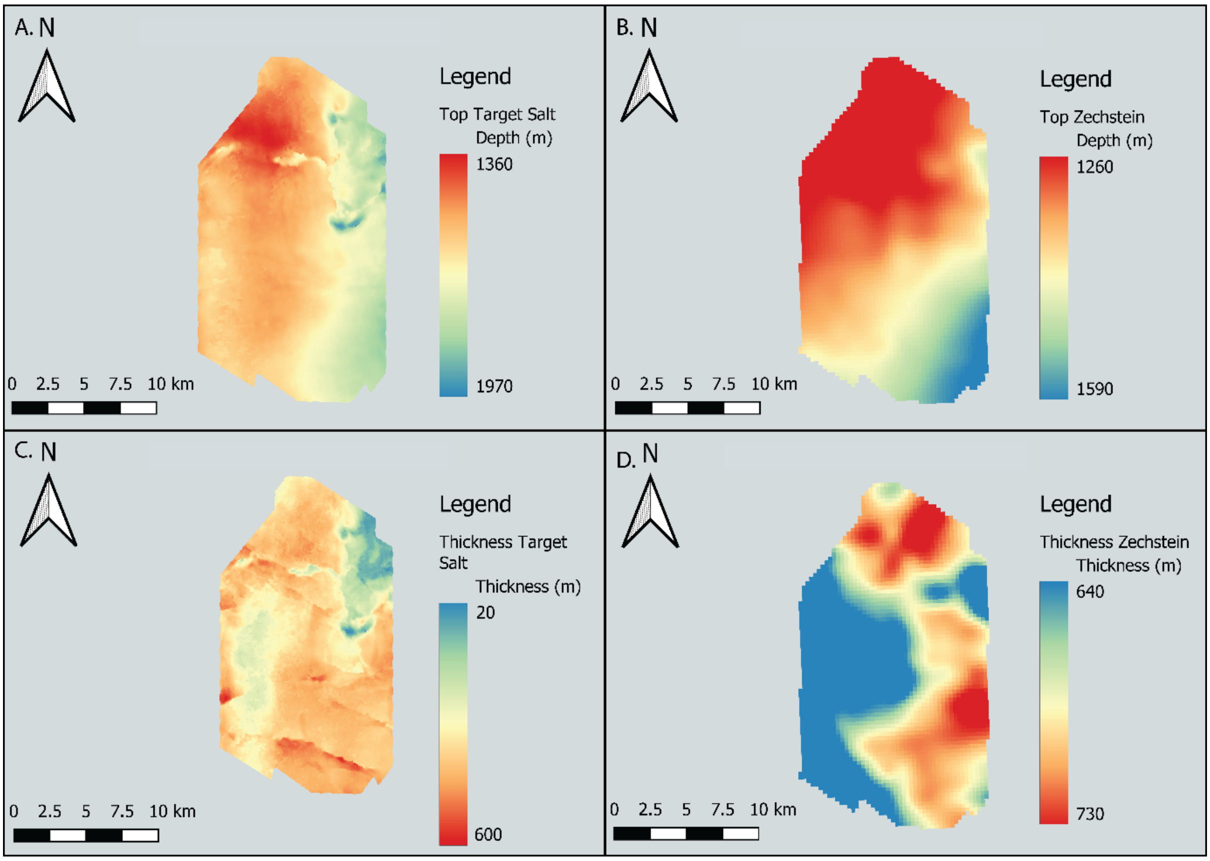

Appendix 2 - Data comparisons between surfaces from ‘Block – Layered Evaporite’ AoI specific geological models (Section 4.4.1-2) basin wide depth surfaces (Section 4.4.3). A and B are depth surfaces, A is for the Top target salt the top Stassfurt halite (Figure. 5), interpreted from seismic data specifically for this study (Used in sections 4.4.1-2), while B is the top Zechstein from the Basin Wide geological model cut to the layered evaporite area (Section 4.4.3), cross sections on seismic data of both surfaces can be seen in Figure. 11. C and D are thickness surfaces, C was calculated from top and base Stassfurt halite interpreted from seismic data, D is the thickness of top and base Zechstein from the Basin Wide geological model.

Appendix 3.

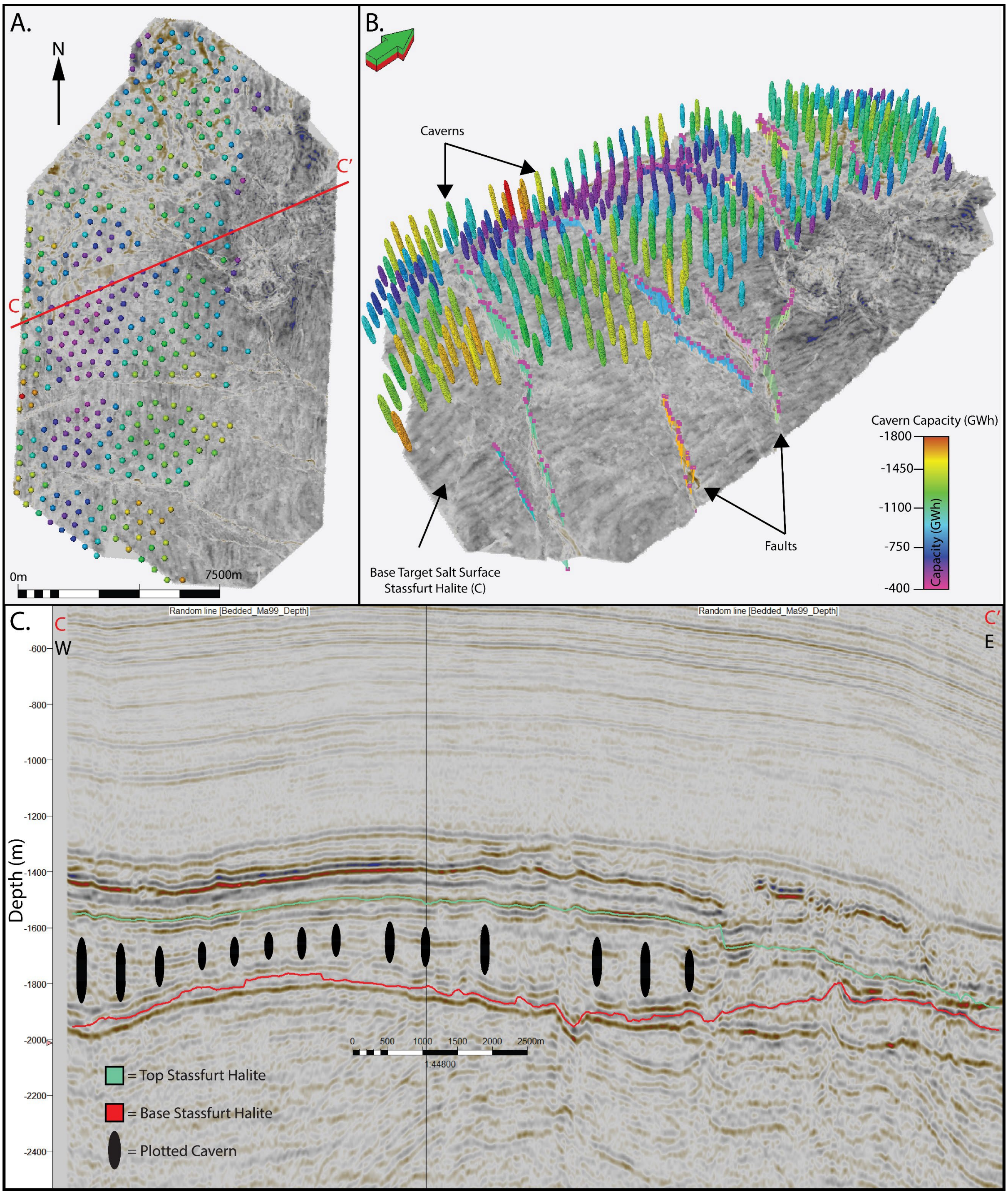

Appendix 3 – Salt caverns within in 3D and 2D space plotted against seismic data (TVD). The salt caverns plotted are the 'Block - Layered Evaporite' AoI with variable caverns (Section 4.4.1). A) Shows caverns coloured for total hydrogen capacity, with the base Stassfurt halite seismic horizon probe surface. B) Shows the same as A, however the camera has been rotated to an angled view, and faults have been displayed on the 3D image, as sticks topped with pink dots. C) A 2d seismic cross-section in TVD (m), C – C’ (Appendix 3, A), running west to east. Top and base Stassfurt halite reflections have been marked on in green and red respectively. Caverns have been plotted in their correct locations. Note how caverns avoid faults.

Best fit algorithm

The best fit algorithm initiates with the list of all viable cavern locations calculated previously in the workflow. Each viable grid cell has an associated cavern and cavern data. The algorithm iterates down the list of viable cavern locations (The spatial order being top left to top right then continuing from the row below again from left to right, finishing in the bottom right of the grid). From the viable caverns, it generates a polygon of equal radius to the required buffer radius depending on the size of the cavern. The buffer polygon is then plotted within the viable area polygon, and checks are made to see if it overlaps with another buffer polygon, if it does overlap, it is removed from the table of viable caverns and the algorithm continues onto the next cavern in the list. The algorithm iterates through every viable cavern location, discarding those that overlap with other caverns. The final product is caverns best fitting within the AOI.

936 **Appendix Distributions**

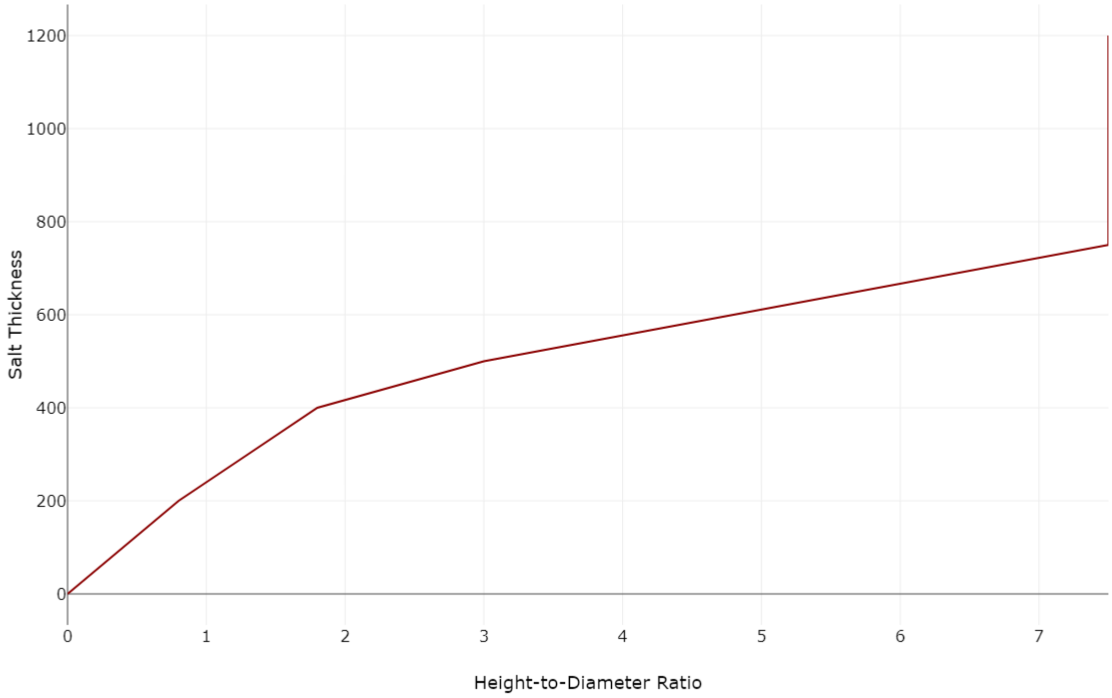

937

938 Distribution 1 – Height-to-diameter ratio pre-set relationship.

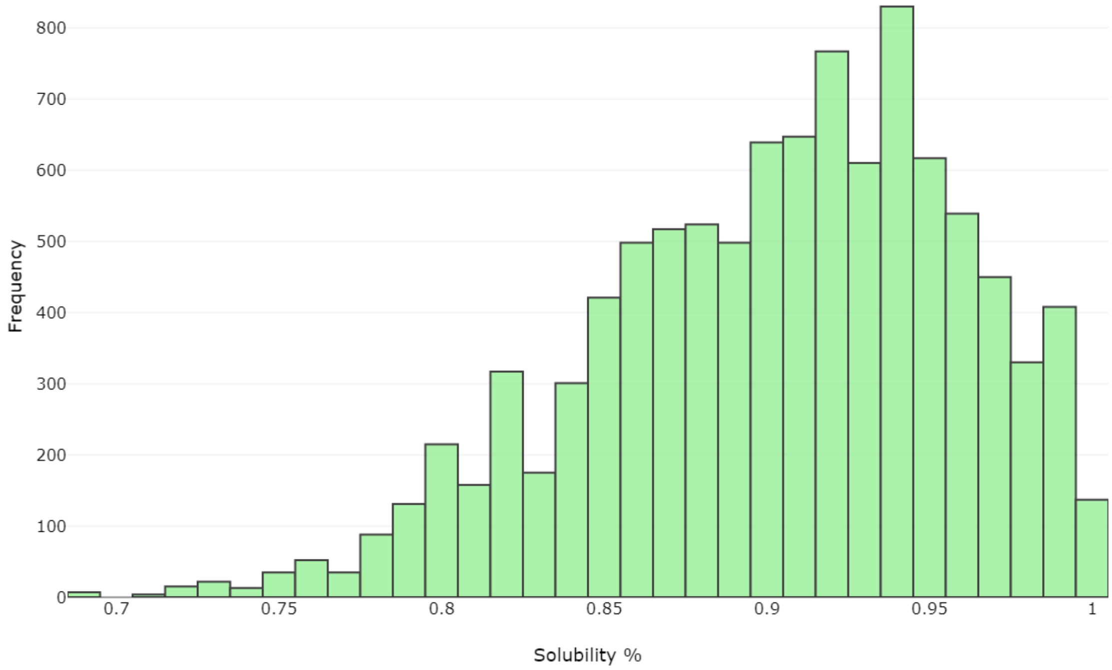

939

940 Distribution 2 – Zechstein Stassfurt halite solubility % distribution within the Southern North Sea

941

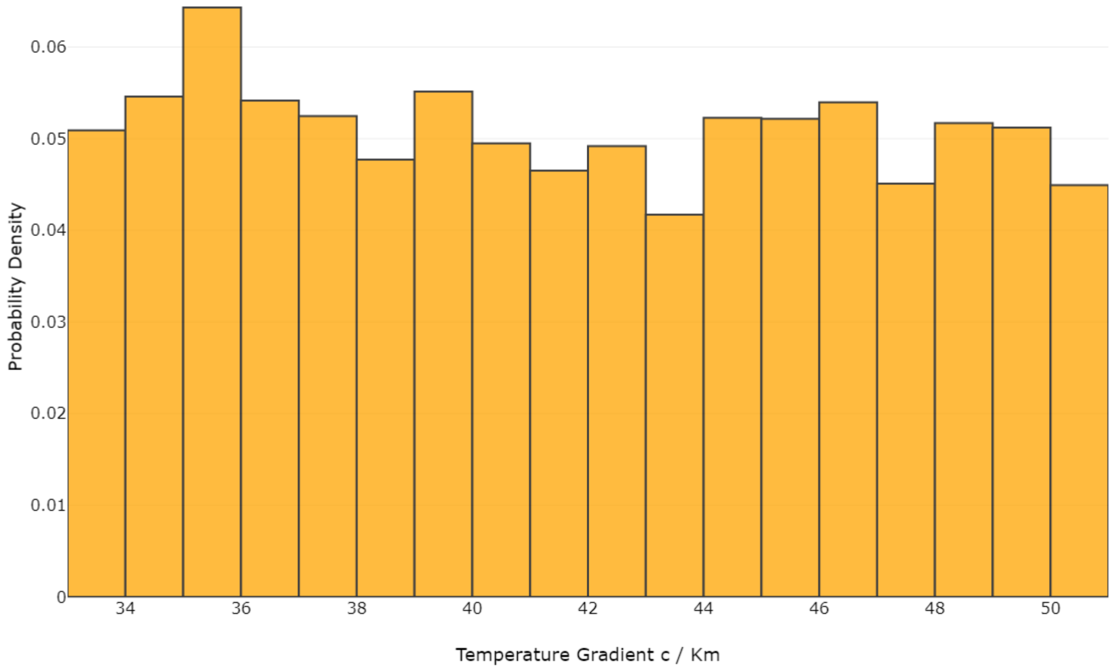

Distribution 3 – Geothermal gradient C / Km used within workflow.

Data Availability

All data generated within this study is available through a data repository located at https://doi.org/10.25405/data.ncl.c.7016283 and is available under a CC BY-SA license. The code/workflow within this study is available under open access licence GPL 3.0+ and can be found as an interactive python notebook either in the data repository or on the primary authors github (https://github.com/Hector-Barn/Tools). The interactive python notebook will be kept-up to date at github. The juypter notebook present within the data repository acts as an archive for the code used within this study for repeatability reasons.

All Montecarlo runs are also available as a CSV file to cross reference shown data and calculated and are available in alongside the geospatial results in the data repo.

The Basin wide surfaces used within this study are available through the following link NSTA Regional surfaces (https://hub.arcgis.com/documents/NSTAUTHORITY::-nsta-and-lloyds-register-sns-regional-geological-mapsa-open-source/about). (Basin wide open licence geological interpretations are available for the Southern North Sea). Seismic survey and well data used are available through the NSTA's National Data Repository (https://ndr.nstauthority.co.uk/)

The CGG geothermal data base used can be found through the following UK gov link (https://www.data.gov.uk/dataset/6cf03f34-12af-41f4-bf9d-1c305a1c5f12/cgg-geothermal-database)

Acknowledgements

Hector Barnett's PhD is funded through the Centre for Doctoral Training (CDT) in Geoscience and the Low Carbon Energy Transition. Seismic and well data were provided by the North Sea Transition Authority under an Open Government Licence. Bathymetry data was provided by The European Marine Observation and Data Network. Data were interpreted using SLB's Petrel and Techlog software which was provided under an academic licence. The code, geological models and outputs from this study are available through data.ncl.ac.uk [https://doi.org/10.25405/data.ncl.c.7016283]

We acknowledge and are grateful to SLB for providing academic licenses for their Petrel and Techlog software which was used to visualise and interrogate the seismic data.

Bibliography

ADAMS, L. & COTTLE, J. 1954. *Underground storage of ammonia and its recovery*. US2901403A.

ALLEN, K. 1972. Eminence Dome - Natural-Gas Storage In Salt Comes of Age. *Journal of Petroleum Technology,* 24**,** 1299-1301.

ALLEN, R. D., DOHERTY, T. J. & THORNS, R. L. 1982. Geotechnical Factors and Guidelines for Storage of Compressed Air in Solution Mined Salt Cavities. *In:* ENERGY, U. S. D. O. (ed.).

ALLSOP, C., YFANTIS, G., PASSARIS, E. & EDLMANN, K. 2023. Utilizing publicly available datasets for identifying offshore salt strata and developing salt caverns for hydrogen storage. *Geological Society, London, Special Publications,* 528**,** 139-169.

ARELLANO-PRIETO, Y., CHAVEZ-PANDURO, E., SALVO ROSSI, P. & FINOTTI, F. 2022. Energy Storage Solutions for Offshore Applications. *Energies,* 15.

BARNETT, H. G., IRELAND, M. T. & VAN DER LAND, C. 2023. Characterising the internal structural complexity of the Southern North Sea Zechstein Supergroup Evaporites. *Basin Research*.

BAUER, S., BEYER, C., DETHLEFSEN, F., DIETRICH, P., DUTTMANN, R., EBERT, M., FEESER, V., GÖRKE, U., KÖBER, R., KOLDITZ, O., RABBEL, W., SCHANZ, T., SCHÄFER, D., WÜRDEMANN, H. & DAHMKE, A. 2013. Impacts of the use of the geological subsurface for energy storage: an investigation concept. *Environmental Earth Sciences,* 70**,** 3935-3943.

BÉREST, P., BROUARD, B., HÉVIN, G. & RÉVEILLÈRE, A. Tightness of Salt Caverns Used for Hydrogen Storage. 55th U.S. Rock Mechanics/Geomechanics Symposium, 2021. ARMA-2021-1616.

BILGILI, M., YASAR, A. & SIMSEK, E. 2011. Offshore wind power development in Europe and its comparison with onshore counterpart. *Renewable and Sustainable Energy Reviews,* 15**,** 905-915.

BOURKE, L., DELFINER, P., FELT, T., GRACE, M., LUTHI, S., SERRA, O. & STANDEN, E. 1989. Using formation Microscanner images: The (Schlumberger) Technical Review.

CAGLAYAN, D. G., WEBER, N., HEINRICHS, H. U., LINßEN, J., ROBINIUS, M., KUKLA, P. A. & STOLTEN, D. 2020. Technical potential of salt caverns for hydrogen storage in Europe. *International Journal of Hydrogen Energy,* 45**,** 6793-6805.

CALADO, G. & CASTRO, R. 2021. Hydrogen Production from Offshore Wind Parks: Current Situation and Future Perspectives. *Applied Sciences,* 11.

CÁRDENAS, B., SWINFEN-STYLES, L., ROUSE, J., HOSKIN, A., XU, W. & GARVEY, S. D. 2021. Energy storage capacity vs. renewable penetration: A study for the UK. *Renewable Energy,* 171**,** 849-867.

CENTRICA. 2023. *Centrica bolsters UK's energy security by doubling Rough storage capacity* [Online]. Available: https://www.centrica.com/media-centre/news/2023/centrica-bolsters-uk-s-energy-security-by-doubling-rough-storage-capacity/ [Accessed 27/09/2023 2023].

CHEN, X.-S., LI, Y.-P., JIANG, Y.-L., LIU, Y.-X. & ZHANG, T. 2022. Theoretical research on gas seepage in the formations surrounding bedded gas storage salt cavern. *Petroleum Science,* 19**,** 1766-1778.

CHEN, X., LI, Y., LIU, W., MA, H., MA, J., SHI, X. & YANG, C. 2018. Study on Sealing Failure of Wellbore in Bedded Salt Cavern Gas Storage. *Rock Mechanics and Rock Engineering,* 52**,** 215-228.

COSTA, P. V. M., COSTA, A. M., SZKLO, A., BRANCO, D. C., FREITAS, M. & ROSA, L. P. 2017. UGS in giant offshore salt caverns to substitute the actual Brazilian NG storage in LNG vessels. *Journal of Natural Gas Science and Engineering,* 46**,** 451-476.

CROTOGINO, F., SCHNEIDER, G.-S. & EVANS, D. J. 2017. Renewable energy storage in geological formations. *Proceedings of the Institution of Mechanical Engineers, Part A: Journal of Power and Energy,* 232**,** 100-114.

DEPARTMENT FOR ENVIRONMENT FOOD AND RURAL AFFAIRS. 2014. *Section_3.2_Temperature_and_Salinity* [Online]. Available: https://webarchive.nationalarchives.gov.uk/ukgwa/20141203184215/http://chartingprogress.defra.gov.uk/feeder/Section_3.2_Temperature_and_Salinity.pdf [Accessed 18/12/2023 2023].

DOORNENBAL, J. C., KOMBRINK, H., BOUROULLEC, R., DALMAN, R. A. F., DE BRUIN, G., GEEL, C. R., HOUBEN, A. J. P., JAARSMA, B., JUEZ-LARRÉ, J., KORTEKAAS, M., MIJNLIEFF, H. F., NELSKAMP, S., PHARAOH, T. C., TEN VEEN, J. H., TER BORGH, M., VAN OJIK, K., VERREUSSEL, R. M. C. H., VERWEIJ, J. M. & VIS, G. J. 2019. New insights on subsurface energy resources in the Southern North Sea Basin area. *Geological Society, London, Special Publications*.

DOWLING, J. A., RINALDI, K. Z., RUGGLES, T. H., DAVIS, S. J., YUAN, M., TONG, F., LEWIS, N. S. & CALDEIRA, K. 2020. Role of Long-Duration Energy Storage in Variable Renewable Electricity Systems. *Joule,* 4**,** 1907-1928.

EISING, J., BROUWER, F. & BERND, A. 2021. *Appendix: Risk analysis of worldwide salt cavern storage.* Vrije Universiteit Amsterdam.

ELAM, S. D. 2007. First Gas after 40 Years – The Geophysical Challenges of the Saturn Gas Complex. *AAPG Annual Convention 2007.* Long Beach, Claifornia.

ELECTRICITY SYSTEM OPERATOR 2023. Future Energy Scenarios. *In:* GRID, N. (ed.).

ENERGY TECHNOLOGIES INSTITUTE 2013. Hydrogen Storage and Flexible Turbine Systems WP2 Report – Hydrogen Storage. *Carbon Capture and Storage - Hydrogen Turbines.*

EVANS, D. J. 2007. An appraisal of Underground Gas Storage technologies and incidents, for the development of risk assessment methodology.

EVANS, D. J. & HOLLOWAY, S. 2009. A review of onshore UK salt deposits and their potential for underground gas storage. *Geological Society, London, Special Publications,* 313**,** 39-80.

FRANÇOIS, L. L. 2021. Four Ways to Store Large Quantities of Hydrogen. *Abu Dhabi International Petroleum Exhibition & Conference.* Abu Dhabi, UAE.

GALLUCCI, M. 2021. The Ammonia Solution: Ammonia engines and fuel cells in cargo ships could slash their carbon emissions. Institute of Electrical and Electronics Engineers.

GILLHAUS, A. 2007. Natural gas storage in salt caverns present trends in Europe Solution Mining Research Institute.

GLENNIE, K. W. 1998. *Petroleum Geology of the North Sea: Basic Concepts and Recent Advances*, Blackwell Scoence.

GRANT, R. J., UNDERHILL, J. R., HERNÁNDEZ-CASADO, J., BARKER, S. M. & JAMIESON, R. J. 2019. Upper Permian Zechstein Supergroup carbonate-evaporite platform palaeomorphology in the UK Southern North Sea. *Marine and Petroleum Geology,* 100**,** 484-518.

HARDWICKE, T. E., MATHUR, M. B., MACDONALD, K., NILSONNE, G., BANKS, G. C., KIDWELL, M. C., HOFELICH MOHR, A., CLAYTON, E., YOON, E. J., HENRY TESSLER, M., LENNE, R. L., ALTMAN, S., LONG, B. & FRANK, M. C. 2018. Data availability, reusability, and analytic reproducibility: evaluating the impact of a mandatory open data policy at the journal Cognition. *Royal Society Open Science,* 5.

HASSANPOURYOUZBAND, A., ADIE, K., COWEN, T., THAYSEN, E. M., HEINEMANN, N., BUTLER, I. B., WILKINSON, M. & EDLMANN, K. 2022. Geological Hydrogen Storage: Geochemical Reactivity of Hydrogen with Sandstone Reservoirs. *ACS Energy Letters,* 7**,** 2203-2210.

HEINEMANN, N., ALCALDE, J., MIOCIC, J. M., HANGX, S. J. T., KALLMEYER, J., OSTERTAG-HENNING, C., HASSANPOURYOUZBAND, A., THAYSEN, E. M., STROBEL, G. J., SCHMIDT-HATTENBERGER, C., EDLMANN, K., WILKINSON, M., BENTHAM, M., STUART HASZELDINE, R., CARBONELL, R. & RUDLOFF, A. 2021. Enabling large-scale hydrogen storage in porous media – the scientific challenges. *Energy & Environmental Science,* 14**,** 853-864.

HEINEMANN, N., BOOTH, M. G., HASZELDINE, R. S., WILKINSON, M., SCAFIDI, J. & EDLMANN, K. 2018. Hydrogen storage in porous geological formations – onshore play opportunities in the midland valley (Scotland, UK). *International Journal of Hydrogen Energy,* 43**,** 20861-20874.

HUNTER, C. A., PENEV, M. M., REZNICEK, E. P., EICHMAN, J., RUSTAGI, N. & BALDWIN, S. F. 2021. Techno-economic analysis of long-duration energy storage and flexible power generation technologies to support high-variable renewable energy grids. *Joule,* 5**,** 2077-2101.

HYUNDER 2013. D3.1 - Assessment of the potential, the actors and relevant business cases for large scale and seasonal storage of renewable electricity by hydrogen underground storage in Europe.

IRELAND, M., ALGARABEL, G., STEVENTON, M. & MUNAFÒ, M. 2023. How reproducible and reliable is geophysical research? *Seismica,* 2.

JACKSON, M. P. A. & HUDEC, M. R. 2017. *Salt Tectonics*, Cambridge University Press.

JAHANBAKHSH, A., LOUIS POTAPOV-CRIGHTON, A., MOSALLANEZHAD, A., TOHIDI KALOORAZI, N. & MAROTO-VALER, M. M. 2024. Underground hydrogen storage: A UK perspective. *Renewable and Sustainable Energy Reviews,* 189.

JOHNSON, WARRINGTON & STOKER 1993. *Lithostratigraphic Nomenclature of the UK North Sea: Permian and Triassic of the Southern North Sea v. 6*, British Geological Survey.

JONES, I. F. & DAVISON, I. 2014. Seismic imaging in and around salt bodies. *Interpretation,* 2**,** SL1-SL20.

KING, M., JAIN, A., BHAKAR, R., MATHUR, J. & WANG, J. 2021. Overview of current compressed air energy storage projects and analysis of the potential underground storage capacity in India and the UK. *Renewable and Sustainable Energy Reviews,* 139.

KUEPPERS, M., PAREDES PINEDA, S. N., METZGER, M., HUBER, M., PAULUS, S., HEGER, H. J. & NIESSEN, S. 2021. Decarbonization pathways of worldwide energy systems – Definition and modeling of archetypes. *Applied Energy,* 285.

LANDINGER, H. & CROTOGINO, F. The role of large-scale hydrogen storage for future renewable energy utilisation. Second International Renewable Energy Storage Conference (IRES II), 2007.

LEITH, W. 2000. Geologic and engineering constraints on the feasibility of clandestine nuclear testing by decoupling in large underground cavities.

LOKHORST, A. & WILDENBORG, T. 2006. Introduction on CO2 Geological Storage - Classification of Storage Options. *Oil & Gas Science and Technology,* 60**,** 513-515.

MA, H., WEI, X., SHI, X., LIANG, X., BAI, W. & GE, L. 2022. Evaluation Methods of Salt Pillar Stability of Salt Cavern Energy Storage. *Energies,* 15.

MCNAMARA, J. W., DEANGELIS, V., BYRNE, R. H., BENSON, A., CHALAMALA, B. R. & MASIELLO, R. 2022. Long-duration energy storage in a decarbonized future: Policy gaps, needs, and opportunities. *MRS Energy & Sustainability,* 9**,** 142-170.

MUHAMMED, N. S., HAQ, B., AL SHEHRI, D., AL-AHMED, A., RAHMAN, M. M. & ZAMAN, E. 2022. A review on underground hydrogen storage: Insight into geological sites, influencing factors and future outlook. *Energy Reports,* 8**,** 461-499.

NATIONAL INSTITUTE OF STANDARDS AND TECHNOLOGY. 2023. U.S Department of Commerce. [Accessed].

NORTH SEA TRANSITION AUTHORITY. 2022. *Gas storage and unloading* [Online]. Available: https://www.nstauthority.co.uk/regulatory-information/gas-storage-and-unloading/#:~:text=Award%20of%20Gas%20Storage%20Licence%20%2D%20July%202022,in%20the%20Southern%20North%20Sea. [Accessed].

OIL AND GAS AUTHORITY 2021. OGA Stratergy.

OZARSLAN, A. 2012. Large-scale hydrogen energy storage in salt caverns. *International Journal of Hydrogen Energy,* 37**,** 14265-14277.

PERYT, T., GELUK, M., MATHIESEN, M., PAUL, J. & SMITH, K. 2010. Chapter 8 Zechstein. *In:* DOORNENBAL, H. & STEVENSON, A. (eds.) *Petroleum Geological Atlas of the South Permian Basin Area.*

PICHAT, A. 2022. Stratigraphy, Paleogeography and Depositional Setting of the K–Mg Salts in the Zechstein Group of Netherlands—Implications for the Development of Salt Caverns. *Minerals,* 12.

ROSMAN, T., BOSNJAK, M., SILBER, H., KOßMANN, J. & HEYCKE, T. 2022. Open science and public trust in science: Results from two studies. *Public Understanding of Science,* 31**,** 1046-1062.

SAMSATLI, S. & SAMSATLI, N. J. 2019. The role of renewable hydrogen and inter-seasonal storage in decarbonising heat – Comprehensive optimisation of future renewable energy value chains. *Applied Energy,* 233-234**,** 854-893.

SEPULVEDA, N. A., JENKINS, J. D., EDINGTON, A., MALLAPRAGADA, D. S. & LESTER, R. K. 2021. The design space for long-duration energy storage in decarbonized power systems. *Nature Energy,* 6**,** 506-516.

SHAN, R., REAGAN, J., CASTELLANOS, S., KURTZ, S. & KITTNER, N. 2022. Evaluating emerging long-duration energy storage technologies. *Renewable and Sustainable Energy Reviews,* 159.

SMDANI, G., ISLAM, M. R., AHMAD YAHAYA, A. N. & BIN SAFIE, S. I. 2022. Performance Evaluation of Advanced Energy Storage Systems: A Review. *Energy & Environment,* 34**,** 1094-1141.

SMITH, N. J. P., EVANS, D. J. & ANDREWS, I. J. 2005. The Geology of Gas Storage in Offshore Salt Caverns. British Geological Survey.

STAFFELL, I., GREEN, R., GREEN, T., JOHNSON, N. & JANSEN, M. 2023. Electric Insights.

STEVENTON, M. J., JACKSON, C. A. L., HALL, M., IRELAND, M. T., MUNAFO, M. & ROBERTS, K. J. 2022. Reproducibility in Subsurface Geoscience. *Earth Science, Systems and Society,* 2.

STROZYK, F. 2017. The Internal Structure of the Zechstein Salt and Related Drilling Risks in the Northern Netherlands.

SUNNY, N., MAC DOWELL, N. & SHAH, N. 2020. What is needed to deliver carbon-neutral heat using hydrogen and CCS? *Energy & Environmental Science,* 13**,** 4204-4224.

SVANBERG, M., ELLIS, J., LUNDGREN, J. & LANDÄLV, I. 2018. Renewable methanol as a fuel for the shipping industry. *Renewable and Sustainable Energy Reviews,* 94**,** 1217-1228.

TAN, Z., ZHANG, Y., NIU, J., WENQI KE, G. C., ZENG, H. & LIU, L. 2021. Construction Progress of Deep Underground Salt Cavern Gas Storage and Challenges of its Drilling and Completion Technology. *E3S Web of Conferences,* 329.

TARKOWSKI, R. & CZAPOWSKI, G. 2018. Salt domes in Poland – Potential sites for hydrogen storage in caverns. *International Journal of Hydrogen Energy,* 43**,** 21414-21427.

TEIXEIRA, L., LUPINACCI, W. M. & MAUL, A. 2020. Quantitative seismic-stratigraphic interpretation of the evaporite sequence in the Santos Basin. *Marine and Petroleum Geology,* 122.

THE ROYAL SOCIETY 2023. Large-scale electricity storage policy briefing.

UK GOVERNMENT 2012. Open Data White Paper Unleashing the Potential.

WALSH, S. D. C., EASTON, L., WANG, C. & FEITZ, A. J. 2023. Evaluating the Economic Potential for Geological Hydrogen Storage in Australia. *Earth Science, Systems and Society,* 3.

WANG, T., YANG, C., MA, H., DAEMEN, J. J. K. & WU, H. 2015. Safety evaluation of gas storage caverns located close to a tectonic fault. *Journal of Natural Gas Science and Engineering,* 23**,** 281-293.

WARREN, J. K. 2006. Evaporites: Sediments, Resources and Hydrocarbons.

WILLIAMS, J. D. O., WILLIAMSON, J. P., PARKES, D., EVANS, D. J., KIRK, K. L., SUNNY, N., HOUGH, E., VOSPER, H. & AKHURST, M. C. 2022. Does the United Kingdom have sufficient geological storage capacity to support a hydrogen economy? Estimating the salt cavern storage potential of bedded halite formations. *Journal of Energy Storage,* 53.

YANG, C., JING, W., DAEMEN, J. J. K., ZHANG, G. & DU, C. 2013. Analysis of major risks associated with hydrocarbon storage caverns in bedded salt rock. *Reliability Engineering & System Safety,* 113**,** 94-111.

ZHANG, G., LIU, Y., WANG, T., ZHANG, H., WANG, Z., ZHAO, C. & CHEN, X. 2021. Pillar stability of salt caverns used for gas storage considering sedimentary rhythm of the interlayers. *Journal of Energy Storage,* 43.

ZHU, S., SHI, X., YANG, C., LI, Y., LI, H., YANG, K., WEI, X., BAI, W. & LIU, X. 2023. Hydrogen loss of salt cavern hydrogen storage. *Renewable Energy,* 218.